International Journal of Chemical Engineering

The 10th International Chemical and Biological Engineering Conference (CHEMPOR 2008)

Guest Editors: Eugénio C. Ferreira and Manuel Mota

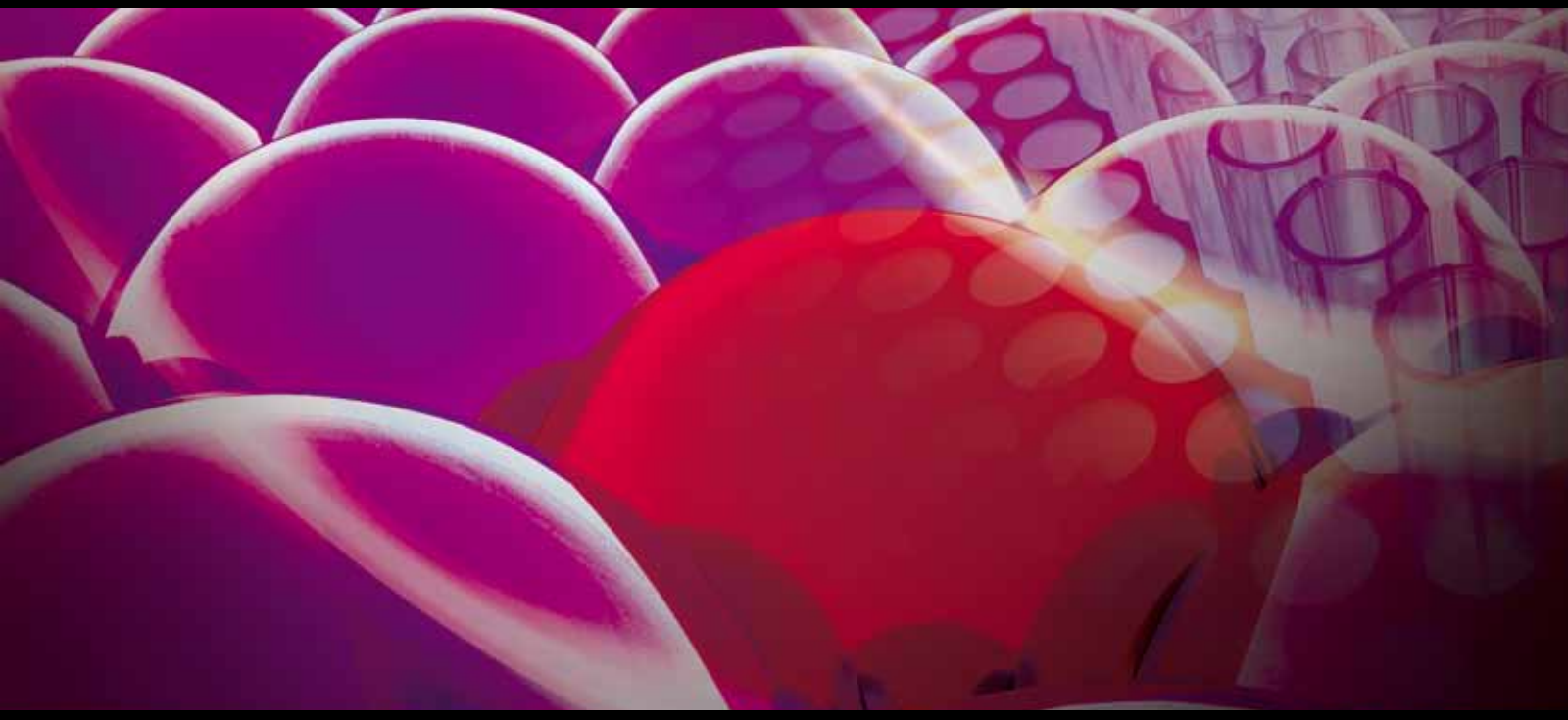

The 10th International Chemical and Biological Engineering Conference (CHEMPOR 2008)

International Journal of Chemical Engineering

The 10th International Chemical and Biological Engineering Conference (CHEMPOR 2008)

Guest Editors: Eugénio C. Ferreira and Manuel Mota

Editorial Board

Contents

Hindawi Publishing Corporation
International Journal of Chemical Engineering
Volume 2009, Article ID 294627, 2 pages
doi:10.1155/2009/294627

Editorial

The 10th International Chemical and Biological Engineering Conference (CHEMPOR 2008)

Eugénio C. Ferreira and Manuel Mota

Institute for Biotechnology and Bioengineering, Centre of Biological Engineering, University of Minho, 4710-057 Braga, Portugal

Correspondence should be addressed to Eugénio C. Ferreira, ecferreira@deb.uminho.pt

Received 25 March 2009; Accepted 25 March 2009

This special issue contains selected papers presented at the 10th International Chemical and Biological Engineering Conference (CHEMPOR 2008), held in Braga, Portugal, from the 4th to the 6th of September, 2008. The conference was jointly organized by the University of Minho, "Ordem dos Engenheiros," and the Institute for Biotechnology and Bioengineeing (IBB), with the support of "Sociedade Portuguesa de Química" and "Sociedade Portuguesa de Biotecnologia."

Thirty years elapsed since CHEMPOR was held at the University of Minho, organized by T. R. Bott, D. Allen, A. Bridgwater, J. J. B. Romero, L. J. S. Soares, and J. D. R. S. Pinheiro. Professors Bott, Soares, and Pinheiro made part of the Honor Committee and were present in this 10th edition. The opening ceremony conferred Professor Bott with a "Long Term Achievement" award acknowledging the important contribution that he brought along more than 30 years to the development of the chemical engineering science, to the launch of CHEMPOR series, and especially his co-operation with the University of Minho.

The CHEMPOR series traditionally brings together both young and established researchers and end users to discuss recent developments in different areas of chemical engineering. The scope of this edition was extended to biological engineering research. One of the major core areas of the conference program was life quality, due to the importance that chemical and biological engineering plays in this area. "Integration of Life Sciences & Engineering" and "Sustainable Process-Product Development through Green Chemistry" were two of the leading themes with papers addressing such important issues. This was complemented with additional leading themes including "Advancing the Chemical and Biological Engineering Fundamentals," "Multi-Scale and/or Multi-Disciplinary Approach to Process-Product Innovation," "Systematic Methods and Tools for Managing the Complexity," and "Educating Chemical and Biological Engineers for Coming Challenges." Papers selected for this special issue represent a good sample of the important themes that were addressed. We wish to thank the authors who have contributed to yield a high scientific standard to this special issue. We also extend our gratefulness to all reviewers through their dedicated efforts that have assisted us in this task.

This special issue contains six papers. Professor Bott's inaugural lecture entitled "Meeting the Challenge" constitutes the first paper. It addresses the importance of the challenge to the scientific community regarding food and water supply for a rapidly growing world population and consequently the need for the effective waste and energy management in processing operations, particularly in the effectiveness of heat recovery and the associated reduction in greenhouse gas emission from combustion processes.

In the second paper entitled "Biofouling Control in Cooling Water," Reg. Bott gives some examples of the effectiveness of different approaches to biofouling control by chemical or physical techniques or a combination of both, and the contribution to the control of greenhouse gas emissions. As stressed by Prof. Bott, unless suitable steps are taken, the accumulation of microbial deposits on the cooling water side of the steam condensers can reduce their efficiency and in consequence the overall efficiency of power production, with an inevitable increase in fuel consumption and hence in CO_2 production.

In the third paper, "Influence of Pyrolysis Parameters on the Performance of CMSM," Campo et al. aimed at understanding the influence of pyrolysis parameters—end temperature, quenching effect, and soaking time—on carbon hollow fiber membrane properties obtained by pyrolysis of a P84/S-PEEK blend. Permeation experiments were performed with nitrogen, helium, and carbon dioxide. Results demonstrated that the highest permeances were obtained for the membrane submitted to an end temperature of 750°C and the highest ideal selectivity for an end temperature of 700°C. Furthermore, it was observed that the membranes quenched after reaching the end of the process revealed higher permeances than the ones naturally cooled.

In the fourth paper, "Influence of Different Cations of N_3 Dyes on Their Photovoltaic Performance and Stability," Andrade et al. investigate the performance and stability of a N_3 dye modified by substituting two of its protons by potassium or sodium cations. Dye-sensitized solar cells incorporating the new dyes were evaluated under light soaking ($1000\,W \cdot m^{-2}$) at 50°C. Photocurrent measurements demonstrated that proton substitution by potassium cations renders the system more stable. Further characterization of the potassium-based devices was performed by electrochemical impedance spectroscopy to investigate the charge transfer phenomena occurring at the different interfaces of the cells.

In the fifth paper is entitled "The kinetics of ampicillin release from hydroxyapatite for bones regeneration" by Ferreira et al. The aim of this work was to evaluate the application of hydroxyapatite as antibiotic delivery carrier. Adsorption kinetic models are compared to describe ampicillin release from hydroxyapatite, a material similar to real bones.

In the sixth paper entitled "Drop Distribution Determination in a Liquid-Liquid Dispersion by Image Processing," Brás et al. present the implementation of an image analysis technique for the automatic identification of drops with different sizes in monochromatic-digitized frames of a dispersion of toluene in water within a transparent mixing vessel. An algorithm is proposed for the calculation of drop size and shape distributions for modelling liquid-liquid systems.

Eugénio C. Ferreira
Manuel Mota

Hindawi Publishing Corporation
International Journal of Chemical Engineering
Volume 2009, Article ID 373784, 5 pages
doi:10.1155/2009/373784

Review Article

Meeting the Challenge

T. Reg Bott

School of Chemical Engineering, University of Birmingham, Edgbaston, Birmingham B15 2TT, UK

Correspondence should be addressed to T. Reg Bott, t.r.bott@bham.ac.uk

Received 25 December 2008; Accepted 17 February 2009

Recommended by Eugénio C. Ferreira

The first Chempor Conference held in Lisbon in 1975 under the auspices of the Calouste Gulbenkian Foundation, heralded a regular wide-ranging review of research and development in Portugal and the UK Progressively in later years the Conferences have attracted contributions from other European countries and indeed further afield. There is an increasing awareness of the problems for the environment, notably global warming, brought about by human activities. Recent predictions about the future are dire, particularly regarding food and water for a rapidly growing world population. They represent a substantial challenge to the scientific and technical fraternity. In response to that challenge it is important to keep up to date with technical developments, to meet and keep in touch with coworkers in associated fields, and to cooperate wherever possible. The papers presented at the Chempor and other conferences have made and continue to make a significant contribution to that objective of meeting the challenge.

1. Introduction

For thousands of years humanity has had to cope and come to terms with the challenges of starvation, disease, and conflict. There have been some useful developments over the years in food production (particularly the so-called "Green Revolution" in the 60s) and in medicine. Sadly though the establishment of universal peace seems as distant as ever. Despite the strides in agriculture and disease control, the basic needs have not been met for a large proportion of the people living in the world. With the anticipated dramatic rise in the population in the coming decades, estimated to be at around eleven billion in 2050, the problems of food production and medical care will become even more intense, unless effective action is taken. The provision of clean water for human consumption is also of vital importance in the suppression of disease. Technology has a responsive role to play in meeting this challenge.

In addition to these basic needs of humanity, energy has played an important part in the lives of many members of the human family since the Industrial Revolution, not only in food production but also in aspects of disease control and particularly in the field of transportation. In previous millennia, energy primarily required for food production was provided either by human or animal power. The phenomenal growth in energy usage generally provided by the heat of combustion of fossil fuels (coal and oil) or other combustible, usually carbonaceous, material has led to the discharge of vast quantities of products from the combustion process, notably carbon dioxide. Although there are dissenters, it is believed by the majority of the informed, that the random discharge of these so-called greenhouse gases to the atmosphere is leading to the phenomenon of global warming, bringing in turn changes to the climate. Additional problems associated with industrialisation and a higher standard of living is waste disposal and satisfactory sanitation.

In a UK government document (a summary of a White Paper) entitled "This Common Inheritance" [1] the following points were made; Mankind long believed that, whatever we did, the earth would remain much the same. We now know that this is untrue. The ways we produce everything and the rate at which we multiply, use natural resources, and produce waste threatens to make fundamental changes in the world environment. Nature is under threat. We have a moral duty to look after our planet and hand it on in good order for future generations. That does not mean trying to halt economic growth. We need growth to give the opportunity to live better and healthier lives.

In recent years, though, the issue of climate change has been paramount in the United Nations, the European Union and individual nations, and various summit gatherings. The Kyoto agreement in 1997 pledged to cut the emission of greenhouse gases principally CO_2 by 12.5% (based on 1990 levels) by 2010. At a recent G8 summit (July 2008) a target of achieving 50% reduction in global emissions by 2050 was suggested. In December, 2007, 15000 people flew to Bali to discuss climate change [2]. It was the intention to build on the achievements of the Kyoto agreement and it was considered to be a success with a continuation of the dialogue begun at Kyoto.

The European Union environmental legislation Integrated Pollution Prevention and Control (IPPC) applies separately to different aspects of the natural environment—air, water, waste, and so on. Porteous [3] states that the IPPC Directive, based mainly on UK law, requires major industrial installations to be licensed in an integrated way for controlling emissions to air and water and the management of waste to protect the environment as a whole. The approach encourages industrialists to think about the whole process adopting cleaner technology rather than just adding "end of pipe" controls.

2. Food Production

One of the major problems of attempting to increase food production to satisfy the growing world population is land use and land availability. Tropical rainforests are constantly burnt and wetlands drained to provide land for agriculture—growing crops and rearing animals as sources of food. The use of land for raising sheep and cattle for food, however, is not considered by many as an efficient use of that land. The opportunity of growing two crops per year of edible foods is much more attractive in the light of the growing number of mouths to feed in the world. Together with pollution of water courses and overfishing, many species of wild plants and creatures are being driven to extinction. As a result valuable sources of food and medicine are lost. The alternative is to improve the output from existing agricultural land, which may be substantially achieved by the application of artificial fertilisers and use of herbicides and insecticides with special safeguards. A recent discourse [4] emphasised that billions of people worldwide suffer from "hidden hunger", an insidious form of malnutrition, that can leave children stunted, immune systems compromised, and adults unable to work effectively. The condition results from micronutrient malnutrition caused by their lack in the diet. The poor in developing countries who live mostly in rural areas depend largely on locally grown staple foods like rice, wheat, and corn to satisfy hunger but these provide insufficient nutrition. A world wide organisation "Harvestplus" is dedicated to the development of staple foods rich in micronutrients that rural populations can grow and consume. In order to provide the necessary content of iron, zinc, and vitaimin A, suitable low-cost fertilisers will be required on a large scale.

3. Water

As important as food, if not more important in many ways, is the availability of clean water. Water supplies around the world are heading towards crisis point. Experts are predicting large-scale water shortages over the next 25 years. It is anticipated that two out of three people on the planet will face regular depletion of water supplies. Population increase and rising standards of living, together with pollution, are rapidly diminishing the availability of naturally occurring sources of clean water. Water-related diseases, such as diarrhoea, cholera, tachoma, hepatitis, and intestinal worms afflict millions of people worldwide. Approximately 1.8 million people die each year from diarrhoeal diseases alone, 90% of whom are children under the age of five [5]. Many pathogens excreted by humans and animals can cause these diseases when they are ingested via faeces-contaminated drinking water. These pathogens and other contaminants can be physically removed by filtering, adsorption, or sedimentation, and they can be rendered innocuous by chemical, heat or u.v treatment.

In developed countries the potable water supply is carefully protected from contamination. In the EU for instance, there are stringent requirements for water quality to safeguard the health of people in respect of microorganisms and toxic substances. Water is usually drawn from rivers or it may be obtained from boreholes in suitable locations by tapping into aquifers. In addtion to serving the public, water has many industrial uses such as a medium for conveyance of wastes, slurries, and wood pulp, as a solvent and as a heat transfer medium principally through vapour (steam), or cooling.

Where sea water is available, desalination becomes a possiblity. In multistage evaporation there are opportunities for efficient energy use and the cosequent implications for global warming. An alternative is the application of reverse osmosis. Koutsakos [6] states that there are not enough chemical engineers employed in this industry.

The disposal of waste water from public sewage systems and industrial use also requires stringent controls, since it is often returned to its source. It has been said that the water in the River Thames is used ten times over in its journey from its source to the sea. In the methods available for the treatment of water the application of physical forces predominate (well known to chemical engineers). In general terms there are three stages. In the treatment of waste water particularly, the primary treatment involves physical operations such as screening and sedimentation that are used to remove the floating and settleable solids from the water. Secondary treatment involves biological and chemical processes to remove organic matter. A final treatment is applied to remove any trace constituents that still remain in the water.

Filtration is widely used for the preparation of public water supplies—including traditional sand filtration and membrane fitration. These have application outside the water industry such as solvent recovery and the production of potable water from sea water. Papers presented at the Chempor Conference in 1975 described the disinfection

of water in the 1974 epidemic of cholera [7] and water demineralisation [8].

4. Waste Disposal

Substantial industrialisation and improved standards of living have given rise to the production of a wide range of waste materials, from manufacturing to domestic and retail outlets. It is usual to classify waste disposal into three categories; landfill, incineration, and recycling. Landfill is subject to tight scrutiny because of the risks to public health, through the contamination of ground water. Disposal at sea, consisting of long-term persistent noxious substances lower the amenity of an area due to smell, visual degradation, and possibly noise, so is not readily acceptable. Flammable waste incineration particularly domestic waste, has been practised for many years. Because of the problem of emissions notably CO_2, the technique has come under critical assessment.

The best option is to recycle, but this is no straightforward option because it is likely to be a mixture of components that may need separation, which can be labour intensive. In order to overcome some of these difficulties it might be possible to recycle in a different way, by the incorporation of plastics and broken bottles in building materials, for instance. At the first Chempor Conference in 1975, Bridgwater and Bessant [9] presented a paper entitled "Plastic waste-disposal or recovery?"

5. Energy

Increased industrialisation and improved living standards that have been achieved in many parts of the world have been largely based on the availability of different forms of energy. The traditional acquisition of energy going back over countless generations has been through combustion to provide heat. Combustion is still an important component in the scheme of things, and is likely to remain so, but the associated technology has become more complex due to the concern for the effects of the associated emissions on the climate, already discussed.

The first priority in achieving minimum output of greenhouse gases is effective energy management. Chemical engineering technology is uniquely placed to make a substantial contribution to effective management to maximise energy efficiency. A basic requirement is effective design, not only in respect to the combustion process itself, but in achieving maximum heat transfer. A recent simplified study [10] of the water-cooled steam condensers on a 550 MW coal-fired power station, demonstrated that a 1 mm thick biofilm on the condensers resulted in an increase of the CO_2 discharged to atmosphere of 6.2 tonne/h. Although this may be considered to be a large additional CO_2 discharge, it represents only a relatively small proportion of the total emission. Nevertheless, if the biofilm formation could be reduced or even eliminated altogether, it would make a significant contribution to reducing the effects of emissions.

Effective control of the accumulation of microbial biofilms can be achieved by the use of biocides. Chlorine has been the preferred biocide for many years on account of its availability and relatively low-cost. Chlorine however represents an environmentally unacceptable pollutant when the water is discharged back to its source. Cooling water is usually taken from a natural source such as a river, lake, or the sea. Under these circumstances the residual chlorine is a danger to living plants and creatures in the water. Furthermore chlorine reacts with organic material to form carcinogenic compounds that are clearly a danger to humans who may come into contact with the water, particularly if it is used for drinking purposes. As a result, alternative, environmentally friendly biocides are available that are continually being improved. The method of dosing, continuous or intermittent, may affect the overall effectiveness of biocide application.

Similarly heat exchangers that recover the heat from hot combustion gases can become fouled with deposits of mineral matter originally contained in the fuel. If steps are not taken to reduce or eliminate these unwanted deposits, the efficiency of heat recovery will be jeopardised, so for a given heat requirement both the fuel consumption will increase and the production of CO_2 will increase.

The reduction of surface fouling in heat exchangers, by good design and suitable control techniques, can make a substantial contribution to a reduction of greenhouse gas discharged to the atmosphere from combustion-based systems. Tackling the problem of heat exchanger surface fouling has been a top technological priority in recent years, particularly since the so-called "oil crisis" in the early 1970s. Improvements to heat exchanger design in respect to fluid velocity and temperature distribution, have made significant contributions to energy conservation. The use of helical baffles in shell and tube heat exchangers [11] and the use of inserts in the tubes [12], to improve the opportunity to remove deposits, are examples of technical advances in design. The material from which a heat exchanger is made and its quality in terms of roughness, have also come under the designers' scrutiny.

Attention to operational managemement to ensure that the design requirements such as flow velocity and temperature distribution are maintained is also an effective tool in maximising energy transfer. The use of modified surfaces and coatings to prevent or reduce surface fouling is also a possibility, although cost and durability have to be carefully considered. The use of additives, as with cooling water, is an option but its presence may not be acceptable in certain products as it may be considered an impurity. This is of particular significance in the processing of food.

In addition to these aspects of energy management, it is possible to reduce emissions by capturing the CO_2 and storing it, usually below ground in deep disused mines and the like. An underground carbon storage facility has recently opened in Australia [13]. The CO_2 originates from a natural gas well, not from a combustion process, but the principle is identical. The storage facility consists of rock formations 2 km below the surface with an estimated capacity of 10,000 tonnes of greenhouse gas. However such a capacity would not be sufficient for a large 1000 MW coal-fired power station that could have around 8 Mt/year CO_2 emission.

The process is most cost effective when applied to large stationary sources of CO_2, such as power stations, refining furnaces, and metal smelting, which account for more than half of all manmade CO_2 emissions. Techniques for capturing CO_2 include absorption, adsorption, and membrane filtration. At the first Chempor Conference in 1975, a paper was presented by Carter et al. [14] entitled "The adsorption of carbon dioxide by deep beds of molecular sieve adsorption". Although this paper was principally concerned with a gas-coolant purification system for a high-temperature nuclear power reactor, it did herald the concept of CO_2 capture for storage underground.

Fossil fuels, particularly oil, are running out, with associated higher costs that have recently been in evidence, so that alternative sources of energy will be required. The combustion of waste, particularly domestic waste, can be a source of energy for power generation, but the emissions that include greenhouse gases may also contain other unwanted compounds, that could be difficult to handle. Preliminary work on the use of hydrogen as an alternative source of energy is a possibility since it does not give rise to greenhouse gas emission from combustion. It may also be used in fuel cells that convert chemical energy directly into electrical energy without combustion. Research is being carried out to investigate their use for powering vehicles. The source of hydrogen in the quantities that will be needed and the fact that it is a gas at atmospheric pressure will create major problems. At the present time hydrogen is largely produced by the electrolysis of water; the source of that power may have come from a conventional power station. Research is being carried out on the possibility of using solar thermo-chemical cycles to produce hydrogen without producing CO_2 [15]. There are however technical problems still to be overcome. An interesting application for industrially generated CO_2, resulting from hydrogen generation is for use in actual greenhouses to encourage plant growth and the capture of CO_2 [16]. Other sources of electrical energy that do not generate greenhouse gases include wind power, solar power, river and tidal barriers, sea wave motion, and geothermal energy.

A developing industry, considered to be a replacement for the combustion of fossil fuels, is the production of "biofuel". It is a fuel as the name implies, which is biological in origin, such as methane, biogas, and biodiesel, seen as sustainable supplements to petrol and diesel. These can be a means of reducing carbon emissions.

Biodiesel refers to a diesel type fluid originating in biological sources such as vegetable oils or animal fats. The manufacturing process produces methyl esters (biodiesel) and a valuable biproduct, glycerine, that has many potential uses. Apart from use in vehicle engines there are other applications such as domestic heating oil to reduce or eliminate the dependence on fossil fuel. Such an application would be of advantage in rural areas where there is no access to domestic gas supplies.

Although combustion generates greenhouse gas emissions, it is argued that since it is plant derived, the CO_2 produced is taken up in subsequent plant growth so that the actual pollution is zero, that is, carbon neutral. An alternative is biomass produced from organic materials directly from plants or from industrial processes. Woody biomass refers to wood-type material or less dense material such as straw and tall grass. Nonwoody biomass as the name implies, includes waste from industrial and food processes and specially grown crops such as sugar cane and maize.

Another alternative is biogas, formed by anaerobic digestion of organic materials, generally waste materials such as sewage sludge and waste from food production. The biogas produced is generally a mixture of methane and carbon dioxide with a ratio of approximately 2:1, respectively. It is possible with suitable modification to use it in internal combustion engines or to generate electricity by the usual method of combustion to raise steam to operate turbines.

In an assessment of the potential for biofuels Bourne Jr. [17] quoting a UN report concludes that although the benefits from biofuels are large, an extensive use of biofuels could jeopardise the security of food supplies, resulting in increased food prices. At the present time it is estimated that 25,000 people die from starvation each day. In the light of these kinds of data it is unfortunate that in some parts of the world rain forests and natural habitats are destroyed to provide areas for the production of crops, which are not for human consumption, but to provide biofuel of one sort or another. Sugar is a typical example. It is fermented to produce alcohol as a liquid fuel to replace petrol in specially adapted internal combustion engines.

A compromise that might go some way to meeting this concern about biofuel and food is to utilise the waste produced in food production and agriculture, rather than using the food substance itself for the production of biofuel. Sugar production from cane is a good example of this approach. For many years waste material from cane sugar refining (bagasse) has been used as a fuel for combustion to produce steam and electricity for the refining process, and the surplus electricity has been made available to the local community. In addtion there is waste associated with the harvesting of the cane on the plantation, currently often burnt in situ. This could also be used as a source of energy. It is anticipated that improvements could make the whole process carbon neutral since the equivalent CO_2 emission would be absorbed by the next year growth.

Green algae, waterborne microorganisms, imbibe CO_2 and provided there is sufficient light available they will rapidly multiply to form a substantial mass of growth. They have often been regarded as a nuisance in reservoirs and in places where there are leisure activities. The Chinese authorities for instance, had to clear vast amounts of algae in preparation for some of the boating competitions at the Olympic Games. It has been suggested that algae might be a good source of biofuel since it is easy to grow and removes greenhouse gas from the environment.

Boyle [18] reports that a company (Ineos) in the UK is proposing to produce bioethanol fuel from municipal solid waste, agricultural waste and organic commercial waste. It is claimed that 400 litres of ethanol could be produced from one tonne of waste. It is pointed out that unlike other biofuels there is no choice to be made between food or fuel with this technology.

6. Concluding Remarks

Humanity is facing a huge challenge in respect of the provision of food and clean water to sustain a rapidly increasing world population. In addition there is the need for energy to satisfy the requirements of the growing population in terms of standard of living and manufacturing industry. The examples cited illustrate the tremendous unique opportunity and indeed the moral obligation for chemical engineers, to apply their skills to meeting this challenge. It is in a spirit of optimism and dedication and the cooperation of governments and industrial entrepreneurs, that will ensure success. The whole process will continue to be facilitated by the exchange of ideas that results from conferences such as Chempor.

References

[1] HMSO, *The Common Heritage*, HMSO, London, UK, 1990.

[2] N. Campbell, "Postcard from bali," *The Chemical Engineer*, no. 801, p. 30, 2008.

[3] A. Porteous, *Dictionary of Environmental Science and Technology*, John Wiley & Sons, Chichester, UK, 4th edition, 2008.

[4] B. McCafferty and Y. Islam, "Fighting the hidden hunger," *The Chemical Engineer*, no. 800, pp. 26–27, 2008.

[5] W. Laursen, "Potters for peace, filters for life," *The Chemical Engineer*, no. 792, pp. 31–33, 2007.

[6] E. Koutsakos, "Thirsting for chemical engineers," *The Chemical Engineer*, no. 804, pp. 26–27, 2008.

[7] A. S. Lobato de Faria, "Influência da protecção sanitária ambiental em especial da desinfecção química da água, na epidemia da cólera de 1974," in *Proceedings of International Chemical Engineering Conference (CHEMPOR '75)*, Lisbon, Portugal, September 1975, paper no. 30.

[8] A. Rodrigues and D. Tondaur, "Desmineralização da água: elementos de cálculo da coluna aniónica," in *Proceedings of International Chemical Engineering Conference (CHEMPOR '75)*, Lisbon, Portugal, September 1975, paper no. 28.

[9] A. V. Bridgwater and J. R. Bessant, "Plastic waste-disposal or recovery?" in *Proceedings of International Chemical Engineering Conference (CHEMPOR '75)*, Lisbon, Portugal, September 1975.

[10] T. Casanueva-Robles and T. R. Bott, "The environmental effect of heat exchanger fouling: a case study," in *Proceedings of 6th International Conference on Heat Exchanger Fouling and Cleaning: Challenges and Opportunities*, H. Müller-Steinhagen, M. Reza Malayeri, and A. Paul Watkinson, Eds., vol. RP2 of *ECI Symposium Series*, Kloster Irsee, Germany, June 2005.

[11] B. Boxma, "Helical baffles in shell and tube heat exchangers," in *Proceedings of the 2nd International Conference on Petroleum Phase Behaviour and Fouling*, pp. P/53.1–P/53.9, Copenhagen, Denmark, August 2000.

[12] A. Wills, T. R. Bott, and I. J. Gibbard, "The control of biofilms in tubes using wire-wound inserts," *The Canadian Journal of Chemical Engineering*, vol. 78, no. 1, pp. 61–64, 2000.

[13] Anon, "CCS: saviour orsmokescreen?" *The Chemical Engineer*, no. 803, p. 3, 2008.

[14] J. W. Carter, H. Hussain, and D. J. Barret, "The absorption of carbon dioxide by deep beds of molecular sieve adsorbents," in *Proceedings of International Chemical Engineering Conference (CHEMPOR '75)*, Lisbon, Portugal, September 1975, paper no. 8.

[15] C. Sattler, M. Roeb, and H. Müller-Steinhagen, "The sun + water = hydrogen," *The Chemical Engineer*, no. 796, pp. 46–47, 2007.

[16] Anon, "IEA GHG meetings in The Netherlands," *Greenhouse Issues*, no. 86, p. 3, 2007.

[17] J. K. Bourne Jr., "Green dreams," *National Geographic Magazine*, vol. 212, no. 4, pp. 38–59, 2007.

[18] C. Boyle, "Rubbish idea that could make driving cheaper," *The Times*, July 2008.

Hindawi Publishing Corporation
International Journal of Chemical Engineering
Volume 2009, Article ID 619873, 4 pages
doi:10.1155/2009/619873

Research Article

Biofouling Control in Cooling Water

T. Reg Bott

School of Chemical Engineering, University of Birmingham, Birmingham B15 2TT, UK

Correspondence should be addressed to T. Reg Bott, t.r.bott@bham.ac.uk

Received 25 December 2008; Accepted 17 February 2009

Recommended by Eugénio C. Ferreira

An important aspect of environmental engineering is the control of greenhouse gas emissions. Fossil fuel-fired power stations, for instance, represent a substantial contribution to this problem. Unless suitable steps are taken the accumulation of microbial deposits (biofouling) on the cooling water side of the steam condensers can reduce their efficiency and in consequence, the overall efficiency of power production, with an attendant increase in fuel consumption and hence CO_2 production. Biofouling control, therefore, is extremely important and can be exercised by chemical or physical techniques or a combination of both. The paper gives some examples of the effectiveness of different approaches to biofouling control.

1. Introduction

The importance of good energy management is becoming far more demanding than in the past. The substantial increase in energy costs and the threat of climate change due to greenhouse gas emissions make it imperative that all steps are taken to reduce energy usage. Of particular importance is the effectiveness of cooling water, specially in the steam condensers of fossil fuel-fired power stations, in maintaining electrical energy output per tonne of fuel at its highest possible level.

Despite efforts to provide an effective design of heat exchanger and careful attention to the maintenance of the design operating conditions, it is likely that fouling on the water side of the heat exchangers will occur unless suitable precautions are taken. The common practice of taking water from natural sources such as rivers and lakes for cooling purposes means that it will contain microorganisms, which will colonise the heat transfer surfaces, to the detriment of cooling efficiency. The problem will be aggravated by the fact that the temperature of the waterside surface in the heat exchanger is usually close to the optimum temperature for maximum microbial growth. In addition water from natural sources will contain nutrients from the breakdown of naturally occurring organic material. Unless this bioactivity is controlled the efficiency of the heat exchanger will be seriously reduced. In fossil fuel-fired power stations this will require additional fuel to be burnt to maintain the required electricity output with an attendant increase in the emission of greenhouse gases. There are basically two methods of controlling this problem, chemical and physical, that might be used separately or in some sort of combination. Three conferences held in Portugal, Melo et al. [1], Melo et al. [2] and International Water Association and Collaborators [3] did much to stimulate interest is these techniques and their effective use. In addition conferences organised byEPI have also covered aspects of the associated technology. The most recent conference was held in Tomar, Portugal in 2007, organised by Müller-Steinhagen et al. [4].

2. Chemical Control

In essence chemical control generally involves the use of biocides to kill the microorganisms in the cooling water, or biostats to reduce their activity. For many years the preferred biocide was chlorine because it was relatively cheap and available. However its use is becoming severely restricted on account of its detrimental effects on the quality of the water discharged back to the natural environment from where it was abstracted and its effect on other living creatures, including humans. In contact with organic material in the natural environment chlorine can form chloromethanes that are carcinogenic. An alternative to the discharge of chlorine-contaminated water is to dechlorinate

before disposal. The techniques for dechlorination are likely to add considerably to the operating costs. As a result efforts are being made to provide alternatives and to be economical in their application. A wide range of chemicals is used as a basis for biocides. They may be classified as oxidising or nonoxidising. Oxidising agents include chlorine and chlorine yielding chemicals, ozone, and hydrogen peroxide. Amongst the nonoxidising compounds are amines, heavy metal compounds, aldehydes, organo-bromine compounds, and isothiazolones.

The so-called "environmentally friendly" biocides are generally those that have a relatively short life after application, breaking down to innocuous products. Simple examples are ozone which reverts to oxygen on decomposition and hydrogen peroxide that breaks down to water. Alternatives to these inorganic chemicals usually involve complex organic compounds that readily breakdown after application. It also has to be appreciated that sometimes these breakdown products are nutrients for microorganisms!.

Clearly the objective is to remove any biofilm as it forms. In order to be economical and effective, the technology of dosing has to be carefully considered. The addition of chemicals to cooling water may be made in three ways.

(a) *Continuous.* The maintenance of a fixed concentration in the circulating water; the dose depending on the concentration and species of the microorganisms present.

(b) *Shock.* An intermittent dose of relatively high concentration maybe only once in 24 hours.

(c) *Pulse.* Involves dosing on a fixed schedule but more frequently than shock dosing maybe once per hour, for example.

The method of dosing will, in general, depend on the season and the quality of the water involved. Careful choice of dosing regime based on trials, preferably in a pilot plant, will help maximise control and minimise cost. It could be beneficial to employ a side-stream test section on the cooling water system to optimise the dosing regime and to make comparisons between alternative biocides.

Some bacteria can develop a potential tolerance to an applied biocide, particularly biocides that affect cell membranes. A change in the dosing regime or a change in the biocide may be effective in overcoming this drawback. Biocides that actually destroy the cell structure are more likely to be the most effective.

In pilot plant studies [5] using *Pseudomonas fluorescens* as the biofllm forming speciesin single tubes, bulk water flow velocities of 0.5 and 1.3 m/s, and a proprietary biocide, the results suggested that pulse dosing, based on comprehensive preliminary testing, is likely to be the most effective regime. This observation is not surprising since pulse dosing is the closest to continuous biocide application.

It is generally considered that the season of the year could affect the accumulation of biofouling since microbial activity will be greatest in the summer when the temperature of the water will be higher than in the other seasons. Some recent work [6] suggests however that it would not be advantageous to modify according to the season, the dosing pattern of 0.2 mg/L chlorine on a 550 MW power station using sea water as the cooling medium.

An alternative to the use of environmentally friendly biocides to meet discharge regulations is to have "zero discharge," that is, to reuse the cooling water, with only "make up" water to replace operating losses. It would allow less costly biocides to be used but nevertheless such a procedure may be costly in maintaining an overall acceptable quality of the circulating water.

3. Physical Control

In theory at least, it should be possible to control biofouling by passing the water through the exchanger at high velocity to increase the removal forces acting on the biofilm. Although this may be feasible, it is not really practical because of the high energy requirement to overcome the large pressure drop involved. There are a number of other physical techniques that may be applied to cooling water systems to reduce the incidence of biofouling, but it has to be said that many are still in the development stage and it remains to be seen if they are practical and economically attractive.

3.1. Circulation of Sponge Rubber Balls. The use of circulating sponge rubber balls with the cooling water through the tubes of steam condensers has been practiced with success, for many years. The balls, having a diameter slightly larger than the internal diameter of the tubes, wipe away any biofilm that begins to form. Cleaning is a random process, so that the concentration of balls in the system has to be sufficiently high so that every tube receives balls frequently enough to ensure effective cleaning. In addition there has to be a replacement policy since the balls lose their effectiveness after a time due to reduced diameter through wear.

3.2. The Use of Inserts. Inserts in tubes, originally intended to boost heat transfer, by the destruction of the laminar sublayer on the tube surface are also capable of reducing the incidence of biofouling at modest water velocities. Two basic types are available: (i) static inserts such as "Hitran" wire wound inserts that break up the laminar sublayer by creating turbulence and associated removal forces at the heat transfer surface and (ii) inserts such as those developed by total, that oscillate in response to the water flow, thereby removing the developing biofilm by abrasion.

Both types of device will increase the pressure drop and hence the operating costs, although this may be offset to some extent by suitable design. Data [7] on the effect of "Hitran" inserts on the accumulation of biofilm consisting of the slime forming species *P. fluorescens* demonstrate that although there is some scatter in the data, it is evident that the presence of the insert reduces the accumulation of biofilm. In one test, after 700 hours operation, the reduction of biofilm accumulation compared to an equivalent test with no insert present was approximately 33% with a water flow velocity of 0.86 m/s and approximately 64% with a water velocity of 1.27 m/s.

Table 1: Control of biofilm formation with different ultrasound treatments.

Amplitude of ultrasound %	Number of 30-second bursts	Frequency of bursts each day	Reduction of biofilm growth compared with no treatment %
20	3	1	20.0
20	3	6	65.5
20	1	8	40.3

Table 2: Mean biofilm thickness over a period of 28 days with different treatments.

Week	Biofilm thickness for different tubes μm	
	Ozone only	Ozone + ultrasound
2	26, 18, 17, 18	9, 8
3	43, 15, 24, 20	11, 12
4	111, 49, 60, 51	7, 5

3.3. The Use of Ultrasound. Ultrasound has the property of disturbing liquids and the structure of solids. It is employed, for instance, to remove hard mineral deposits from heat exchange surfaces exposed to high temperature combustion gases in boiler installations. It has been demonstrated experimentally [8] that biofilm accumulation (*P. fluorescens*) on the inside of tubes can be reduced by the modest use of ultrasound of 20 kHz. Depending on the amplitude (20 or 40%), the length (time), and frequency of groups of bursts of ultrasound, the reduction in biofilm accumulation varied between 20 and 93%. The water flow velocity was 1 m/s. Some further detail is given in Table 1.

A major drawback in respect of the use of ultrasound for the control of biofouling is the initial cost of the equipment and its inclusion in heat exchanger design.

3.4. Circulation of Polymer Fibres. Some preliminary work [7] on the use of Aramid fibres to control biofouling suggests that the technique could be useful. Again using *P. fluorescens* as the biofouling bacterium, it was shown that a concentration of fibres of 100 ppm with a water velocity of 1.6 m/s is adequate for effective control of biofilm formation. It was noteworthy that if fibre addition was stopped, a biofilm soon began to form. Considerably more work on the technology will be required however, before it can be applied effectively to industrial cooling water. A major difficulty that would have to be faced would be the recovery of the fibres prior to the final discharge of the water. Fibre removal might also be necessary before passing the water through a cooling tower in a recirculation system, to avoid potential accumulation and associated blockage problems. Some preliminary work suggests that the fibres do not accelerate the wear on the associated pumps.

4. Combined Chemical and Physical Control

It is possible that a combination of chemical and physical techniques of control could be more effective than either solely applied.

4.1. Ozone and Ultrasound. Experimental work using a combination of ozone and ultrasound over a four-week period [9], again using *P. fluorescens* as the biofilm former and a water velocity of 1 m/s demonstrated that this was a more effective control than ozone alone. During the first week of a four-week period, no treatment was applied to allow a biofilm to develop. The biofilm thickness at the end of that first week ranged from 45–60 μm. Table 2 presents some of the data obtained during the subsequent three weeks, demonstrating that the application of the ultrasound (20 kHz at 20% amplitude) for three minutes each day made a considerable difference to the retention of biofilm. The ozone concentration in the water during these tests was very low, since water containing an ozone concentration of around 2.2–2.8 mg/L was pumped into the system to be mixed with the bulk water for only three hours each day. The data contained in Table 2 indicate that the application of ultrasound made a considerable reduction in the accumulated biofilm.

4.2. Propriety Biocide and Inserts. Limited results [10] using Hitran inserts in conjunction with a propriety biocide have demonstrated that whereas a biocide concentration of around 50 mg/L would normally be required to control biofilm formation, in the presence of inserts, the concentration required could be as low as 10 mg/L. The conditions of these tests were similar to those quoted elsewhere in this paper.

5. Concluding Remarks

This brief summary of investigations into the factors that influence biofilm formation and perhaps more importantly the opportunities for control of biofilm growth demonstrate how the application of chemical engineering and associated technologies can help meeting the challenge of climate change and the associated impact on the well-being of humanity.

Conferences such as Chempor do much to spread the word about what is possible through the application of chemical engineering principles. Furthermore the "networking" that is a direct result of conference attendance is extremely valuable in that it facilitates a combined approach to meeting the challenge.

References

[1] L. F. Melo, T. R. Bott, and C. A. Bernardo, *Fouling Science and Technology*, Kluwer Academic Publishers, Dordrecht, The Netherlands, 1988.

[2] L. F. Melo, T. R. Bott, M. Fletcher, and B. Capedeville, *Biofilms Science and Technology*, Kluwer Academic Publishers, Dordrecht, The Netherlands, 1992.

[3] International Water Association and Collaborators, International Specialised Conference on Befouling Monitoring, 2000.

[4] H. Müller-Steinhagen, M. Reza Malayeri, and A. P. Watkinson, Eds., *Heat Exchanger Fouling and Cleaning VII*, Engineering Conferences International, Tomar, Portugal, July 2007.

[5] D. M. Grant and T. R. Bott, "Biocide dosing strategies for biofilm control," *Heat Transfer Engineering*, vol. 26, no. 1, pp. 44–50, 2005.

[6] T. Casanueva Robles, *Estudio y Control del Biofouling Marino en Tubes de Latón-aluminio y Titanio. Aplicación al Condensador de una Central Térmica*, Ph.D. thesis, University of Cadiz, Cadiz, Spain, 2009.

[7] T. R. Bott, "Potential physical methods for the control of biofouling in water systems," *Chemical Engineering Research and Design*, vol. 79, no. 4, pp. 484–490, 2001.

[8] T. R. Bott, "Biofouling control with ultrasound," *Heat Transfer Engineering*, vol. 21, no. 3, pp. 43–49, 2000.

[9] T. R. Bott and L. Tianqing, "Ultrasound enhancement of biocide efficiency," *Ultrasonics Sonochemistry*, vol. 11, no. 5, pp. 323–326, 2004.

[10] A. M. Wills, T. R. Bott, and I. Gibbard, "The effect of tube inserts on biocide efficacy," in *Heat Exchanger Fouling. Fundamental Approaches and Technical Solutions*, H. Müller Steinhagen, Ed., Publico, Essen, Germany, 2002.

Hindawi Publishing Corporation
International Journal of Chemical Engineering
Volume 2009, Article ID 147879, 7 pages
doi:10.1155/2009/147879

Research Article

Influence of Pyrolysis Parameters on the Performance of CMSM

Marta C. Campo,[1] Tymen Visser,[2] Kitty Nijmeijer,[2] Matthias Wessling,[2] Fernão D. Magalhães,[1] and Adélio M. Mendes[1]

[1] *Laboratory of Process, Environment and Energy Engineering (LEPAE), Chemical Engineering Department, Faculty of Engineering, University of Porto, 4200-465 Porto, Portugal*
[2] *Membrane Technology Group (MTG), Faculty of Science and Technology, University of Twente, 7500 Enschede, The Netherlands*

Correspondence should be addressed to Adélio M. Mendes, mendes@fe.up.pt

Received 1 October 2008; Revised 29 January 2009; Accepted 11 March 2009

Recommended by Eugénio C. Ferreira

Carbon hollow fiber membranes have been prepared by pyrolysis of a P84/S-PEEK blend. Proximate analysis of the precursor was performed using thermogravimetry (TGA), and a carbon yield of approximately 40% can be obtained. This study aimed at understanding the influence of pyrolysis parameters—end temperature, quenching effect, and soaking time—on the membrane properties. Permeation experiments were performed with N_2, He, and CO_2. Scanning electron microscopy (SEM) has been done for all carbon hollow fibers. The highest permeances were obtained for the membrane submitted to an end temperature of 750°C and the highest ideal selectivities for an end temperature of 700°C. In both cases, the membranes were quenched to room temperature.

1. Introduction

Carbon molecular sieve membranes (CMSMs), pioneered by Koresh and Soffer in the 80s, are a very recent research topic in the area of gas separation. These inorganic materials present great advantages over polymeric membranes, since they have comparatively high permeabilities and selectivities, together with high thermal and chemical stability [1–4]. The main applications for this type of membranes are, among others, air separation, landfill gas recovery, olefin/paraffin separation, hydrogen recovery, and natural gas processing.

Carbon membranes are produced by pyrolysis of a polymeric precursor under an inert atmosphere [1, 3]. The main precursors mentioned in literature are, among others, polyimide, polyfurfuryl alcohol polyacrylonitrile, phenolic resins, and cellulose [3]. The precursor material should have a high-carbon yield and be thermosetting [2]. To further improve the separation capacity of CMSM, some authors have functionalized the carbon matrix by adding metals with affinity towards one of the permeating species [5]. This strategy was followed by Barsema et al. [6, 7]. These authors used a blend of P84/AgS-PEEK to produce flat sheet carbon membranes and determined the influence of Ag on the membranes' separation performance. However, the influence of the pyrolysis end temperature, soaking time or cooling procedure was not assessed. In the present work, a P84/SPEEK blend is used for the first time as a hollow fiber precursor for preparing carbon membranes and to study the influence of some of the pyrolysis parameters on the final performance. The hollow fiber configuration provides higher mechanical stability than flat sheet membranes.

The preparation of CMSM should be directed towards the tailoring of the final carbonaceous micropore network. The influence of the pyrolysis parameters and complementary treatments used for producing the final carbon membranes should be studied in order to better suit a certain application [1, 8]. Examples of these complementary treatments are pore closing by carbon vapor deposition using a carbon-containing source, or pore widening by activation under an oxidative atmosphere [3, 9–11]. The temperature programs followed in the pyrolysis, the cooling steps and the gas atmosphere employed, are all important aspects that have to be studied and optimized according to the selected precursor, having in mind the final application.

CMSMs have two major disadvantages that still have to be overcome: mechanical brittleness and aging effects [4, 12]. Aging is caused by oxygen chemisorption on the carbon surface, which reduces the membrane performance due to reduction of pore size [12]. The presence of oxygenated functional groups on the surface of CMSM was reported by other authors [12–14]. The resulting adsorption of species with affinity to these oxygenated functional groups such as CO_2 may also contribute to this fact [15]. When the feed mixture is humidified, the oxygen content on the carbon matrix may lead to the adsorption of water vapor, which may block the passage of other species [16]. In this work the use of P84/SPEEK hollow fibers is suggested for overcoming these problems. Evidences of aging effects will also be looked for in carbon membranes out of this precursor.

2. Experimental

2.1. Materials and Precursor Preparation. The precursor asymmetric hollow fiber membranes were prepared from a blend of 3.5 wt% S-PEEK and 96.5 wt% P84. P84 (BTDA-TDI/MDI) is a commercial available copolyimide from Lenzing, and S-PEEK is custom made polymer obtained by sulphonation of poly (ether ether ketone) (PEEK, Victrex). A few % of S-PEEK in the blend introduces additional hydrophilicity and may help suppressing macrovoids in spinning fibers. The P84/S-PEEK hollow fibers were obtained by the dry/wet phase separation process using spinning technology. For this purpose the dope used consisted of 71% of NMP (N-methyl-pyrrolidone, Merck 99%), and 18% P84/S-PEEK blend. Additives were 6 wt% polyvinylpyrrolidone (PVP K90, Acros) and 5 wt% glycerol (Merck >99%), and the coagulant medium was tap water. In order to induce pore formation on the inside and outside skin, a bore and shell liquid were used with, respectively, 80/20 and 90/10 wt% NMP/H_2O. An air gap was used of 20 mm, and the fibers were spun at room temperature. More details about the spinning process can be found elsewhere [17, 18].

2.2. Thermogravimetric Analysis of Precursor. The precursor used in this study was a copolyimide P84/S-PEEK blend. The thermogravimetric proximate analysis performed is a method developed by Ottaway [19] to determine the moisture, volatile matter, fixed carbon, and ash contents of a sample. The heating procedure consists on rising the temperature at 25°C min^{-1} under nitrogen, with dwelling times at 50 and 110°C (10 and 7 minutes, respectively) and at 950°C (9 minutes under nitrogen plus 11 minutes under oxygen). After the second dwell at 110°C, humidity is removed. Up to the third dwell, under nitrogen, volatile matter is released. Finally, after 11 minutes under oxygen at 950°C, all the fixed carbon is lost, yielding ashes, if existent.

The proximate analysis of the precursor was performed in a Netzsch TG 209 F1 Iris thermogravimetric balance.

2.3. Fabrication of Carbon Hollow Fiber Membranes. The pyrolysis occurred inside a quartz tube installed in a Carbolite TZF 12/100 High Temperature Tubular Furnace

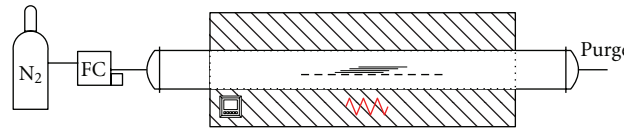

Figure 1: Scheme of the pyrolysis set-up.

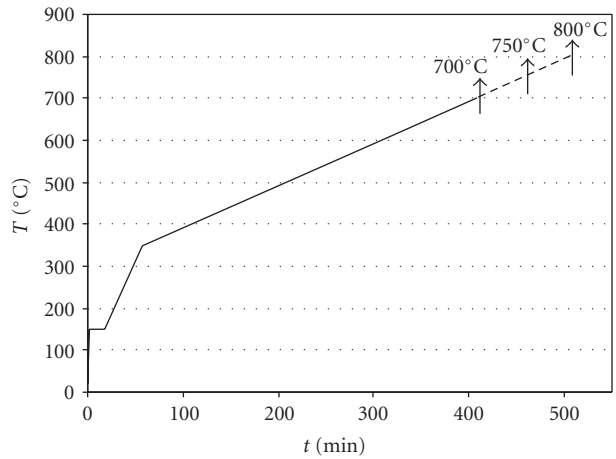

Figure 2: Heating procedure to prepare carbon membranes based in literature [6, 7].

with a Eurotherm 2408 CP temperature controller, under a 50 $ml_N \cdot min^{-1}$ nitrogen atmosphere. The hollow fibers were supported on a stainless steel grid and introduced into the furnace with a cane as illustrated in Figure 1.

The temperature program employed is based on a program developed by Barsema et al. [6, 20] and shown in Figure 2. The membranes were heated from room temperature up to 150°C at 50°C min^{-1}, remaining 15 minutes at this temperature. This step allowed the removal of any possible adsorbed water or residual solvents. Thereafter, the membranes were heated up to 350°C at 5°C min^{-1}. The heating rate up to the final temperature was then 1°C min^{-1}. This low heating rate prevents cracks from occurring during the formation of the carbon matrix. After achieving the maximum temperature of pyrolysis, here designated as end temperature, the membranes were submitted to quenching or to natural cooling. In some cases, they were kept at the end temperature for a certain time before cooling (soaking step). The main differences from Barsema's protocol relate to the end temperature, quenching procedure, and soaking time.

The quenching consisted on fast cooling inside a jacketed container, refrigerated with cold tap water, under nitrogen. "*No*" quenching means that the sole driving force for cooling was the temperature difference between the inside of the furnace and the surrounding room atmosphere. The transfer of the carbon hollow fibers from the furnace into the quenching container was performed as fast as possible, in order to minimize air exposure. Afterwards the membranes were stored in a box flushed with nitrogen.

The influence of a final step—soaking time—in which the oven end temperature was kept constant for 2 hours before quenching was also analysed.

Table 1: Identification of the samples and pyrolysis' parameters.

Sample	T_{END} (°C)	Soaking time (h)	Quenching
HF-700-A	700	0	Yes
HF-700-B	700	0	No
HF-750-A	750	0	Yes
HF-750-B	750	0	No
HF-800-A	800	0	Yes
HF-800-B	800	0	No
HF-700-ST2h	700	2	Yes

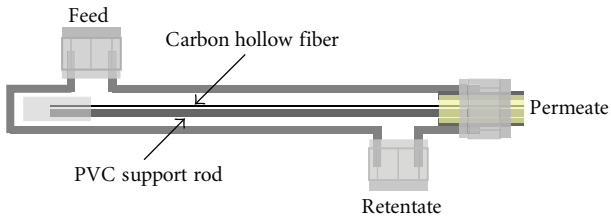

Figure 3: Scheme of the membrane module.

These two steps, soaking and quenching, may probably lead to microstructural rearrangements, affecting the pore size distribution and, consequently, the membrane selectivity.

Table 1 shows the identification of each carbon membrane prepared, concerning its pyrolysis' parameters.

2.4. Scanning Electron Microscopy. All samples identified in Table 1 were characterized by means of scanning electron microscopy using a JEOL JSM 5600 LV SEM; the fibers were fractured and the cross-sections analyzed. All the samples were previously sputtered with gold using a Balzers Union SCD 040 to allow better conductivity for SEM. Through the pictures taken it was possible to measure the thickness, ℓ, of the selective layer located in the fiber bore side, the inner and outer diameters of each fiber, D_{in} and D_{out}, and consequently the wall thickness, ℓ_w. This information, together with the length of the carbon hollow fiber, L, allowed the calculation of the effective area of the selective layer of the membrane, A_m.

2.5. Permeation. After pyrolysis, the resulting carbon membranes were assembled in a module. Figure 3 illustrates the membrane module, where it is evidenced that feed circulates in the shell side, whereas permeate is removed from the bore side. These individual modules were then connected to a stainless steel housing which was introduced in a temperature controlled cabinet.

The permeation experiments were conducted at 30°C, using a pressure increment method. The several carbon membranes were tested towards N_2, He, and CO_2. All the modules were submitted to a 2 bar feed pressure on the shell side; whereas vacuum was applied on the bore side. Here, ideal gas behavior was assumed and, hence, the monocomponent permeance P/ℓ was calculated according to

$$\frac{P}{\ell} = \frac{V_P \upsilon_M \left(p_l^t - p_l^0\right)}{\Re T t A_m (p_h - p_l)}, \quad (1)$$

where V_P is the volume of the tank where the permeate is collected, p_l and p_h are, respectively, the permeate pressure and the feed pressure, A_m is the effective area of the fiber, T is the absolute temperature, υ_M is the molar volume of the gas, $\Re$ is the gas constant, and t is the time. The ideal selectivity $\alpha_{i/j}$ for a certain pair of gases i and j is obtained from

$$\alpha_{i/j} = \frac{P_i}{P_j}, \quad (2)$$

where P_i and P_j are the permeabilities of species i and j, respectively.

3. Results and Discussion

3.1. Thermogravimetry. Proximate analysis is normally performed in order to determine the percentage of humidity, volatile matter, fixed carbon, and ashes [19]. The most important variable in this study is the yield of fixed carbon. This percentage accounts for the carbon content of the final carbon membrane. Higher fixed carbon content indicates that the resultant membranes have the potential to become more mechanically stable. Yields of fixed carbon are usually in the range of 25–50%, depending on the precursor material [21]. Figure 4 presents the results of the proximate analysis. The normalized sample mass is represented as a function of time, and the heating procedure is referred to the secondary axis. The yield of fixed carbon is determined from the difference between the final mass and the mass at 63 minutes, being approximately 40%. In the literature some polymers are reported to have carbon yields of almost 60% [22]. However, the result of 40% for P84/S-PEEK blend can still be considered quite good. Probably due to the high P84 content in the blend, this value is similar to those reported in the literature for P84 alone [20, 23].

It is known that S-PEEK and P84 have different thermal stabilities, but it is difficult to distinguish the precise contribution of each component for the shape of the thermogravimetric curve. Nevertheless, the first slope around 200°C should be caused by the degradation of the sulphonic acid group present in S-PEEK. Around 400°C, a new slope is observed, due to the degradation of P84 [23]. Since the polymeric chain of S-PEEK decomposes at about 550°C, this might be the cause for the final slope [24].

3.2. Scanning Electron Microscopy. SEM pictures were taken to compare the structures of the different samples. The pyrolysis operating variables, such as, end temperature, soaking time, and natural cooling procedure, have affected the dimensions of all studied fibers. Besides that, no other considerable changes are observed through SEM. Figure 5 provides an example of micrographs taken for sample HF 700B. This membrane was pyrolysed up to 700°C and

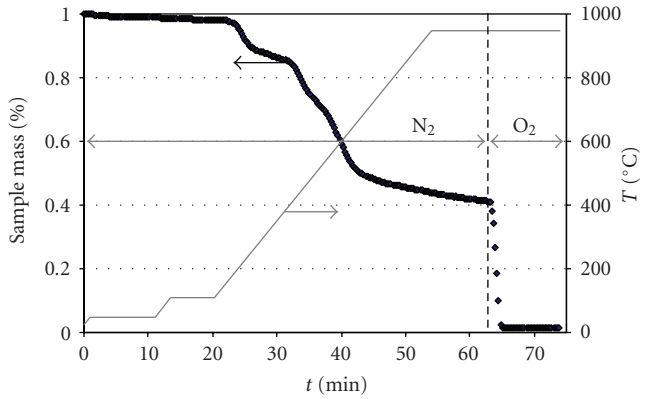

Figure 4: Typical sample mass and temperature histories during proximate analysis procedure.

naturally cooled. Table 2 summarized the dimensions of all carbon membranes studied.

It is seen that an increase in the pyrolysis end temperature originates a decrease of the inner and outer diameters of the fibers. This fact is sustained by the results of the proximate analysis, presented in Figure 4, which show that between 700 up to 800°C mass loss still occurs, as volatile matter is still being released. It is during this stage that heteroatoms are set free that the pore network is created. Also in Table 2, but regarding the A/B pairs pyrolysed at the same end temperature but with different cooling procedures, it is noticeable that the nonquenched membranes have lower diameters. This may be related to higher mass loss and rearrangement of the carbon matrix occurring during the slow cooling. In agreement with these results, the membrane kept for 2 hours at 700°C before quenching (HF-700-ST2h) shows smaller dimensions than the one quenched with no soaking time (HF-700-A).

3.3. End Temperature Effect. The effect of the end temperature on the performance of carbon hollow fiber membranes can be studied by determining monocomponent permeances. Table 3 lists permeances and ideal selectivities for samples pyrolysed up to 700, 750, and 800°C towards N_2, He, and CO_2. These results are plotted in Figure 6.

These results show that the membrane prepared with a 750°C end temperature displays the highest permeance towards all the species studied. For all the membranes, the species with lower permeance is N_2, the species with larger size (Lennard-Jones kinetic diameter 0.364 nm). On the other hand, CO_2 has higher permeance than He, despite its larger kinetic diameter (0.33 nm and 0.26 nm, resp.). However, it is known that CO_2 has high adsorption affinity towards carbon matrixes, in opposition to He, which mostly does not adsorb. It is being assumed that adsorption plays a significant role in the mass transport mechanism through these membranes: molecular sieving combined with activated diffusion.

The highest ideal selectivity values are achieved for an end temperature of 700°C. The increase in permeances observed for all species when the temperature increases

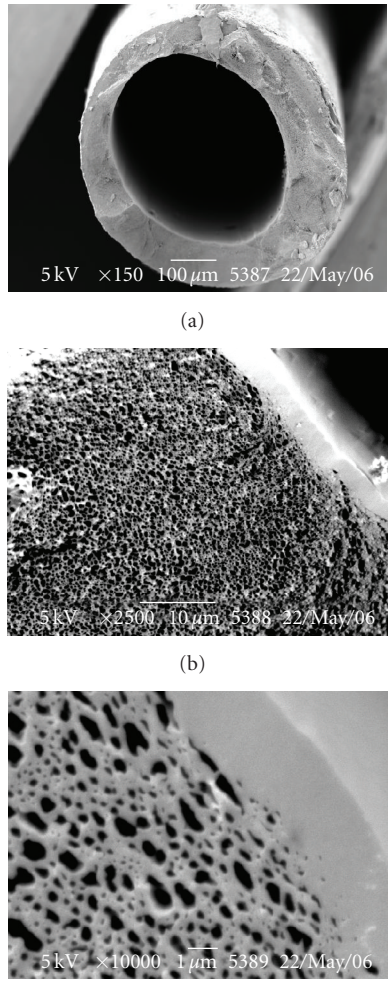

Figure 5: SEM pictures from HF-700-B carbon hollow fiber membrane cross-sections: (a) global view, ×150 magnification, (b) inner view, ×2500 magnification, and (c) inner view, ×10 000 magnification.

to 750°C might indicate that the total pore volume has increased, in the sense that more path ways are created enhancing the transport of the species. On the other hand, the decrease in selectivity for the pairs CO_2/N_2 and He/N_2 suggests that the mean pore width is also increasing, which impairs the sieving effect. At 800°C end temperature sintering mechanisms explain the decrease in permeances [2, 10, 25].

3.4. Quenching Effect. In this study, as previously mentioned, it was intended to analyze the permeance dependency on the way membranes are cooled from the pyrolysis end temperature to room temperature. Table 4 summarizes the permeation data and ideal selectivities of the membranes obtained at different end temperatures from 700 up to 800°C.

For each end temperature, the quenched membranes show larger permeances over the ones that were slowly cooled. This qualitatively indicates that the total pore volume

Table 2: Characteristics of the carbon membranes.

Sample	D_{in} (μm)	D_{out} (μm)	ℓ_w (μm)	ℓ (μm)	L (cm)	A_m (cm^2)
HF-700-A	401	600	199	3.2	6.9	0.87
HF-700-B	397	588	190	3.1	6.4	0.80
HF-750-A	386	583	197	2.8	6.4	0.78
HF-750-B	387	570	183	2.8	7.5	0.91
HF-800-A	366	562	196	2.7	5.3	0.61
HF-800-B	356	536	180	2.9	6.3	0.70
HF-700-ST2h	397	585	188	2.8	5.4	0.67

Table 3: Effect of end temperature on the permeance of carbon hollow fibers.

	Permeance ($10^{-8} \times m^3_N\, m^{-2}\, kPa^{-1}\, s^{-1}$)			Ideal selectivity		
Sample	N_2	He	CO_2	CO_2/N_2	CO_2/He	He/N_2
HF-700-A	9	107	153	18	1.5	12
HF-750-A	28	176	416	15	2.4	6.4
HF-800-A	14	97	144	10	1.5	7.0

created during the heat treatment is maintained when the membrane is quenched. On the other hand, slow cooling allows for structural rearrangement of the carbon graphene layers, leading to pore narrowing. In the case of the carbon membranes prepared at 700°C, the He/N_2 selectivity is higher for the naturally cooled membrane. Furthermore, the fact that the CO_2/He selectivity turned smaller than unity indicates that the pore width has decreased together with the pore volume, revealing the onset of a molecular sieving effect towards CO_2. It is also observed that the highest permeances are generically obtained when the membranes are quenched just after reaching 750°C. For 750°C, the quenching effect essentially affects the permeance and not the selectivities. Concerning the membranes prepared at 800°C, the selectivities have decreased with quenching, except for the pair He/N_2. The pore volume and the pore width are disfavoring the permeation of the more adsorbed species, that is, CO_2 and N_2.

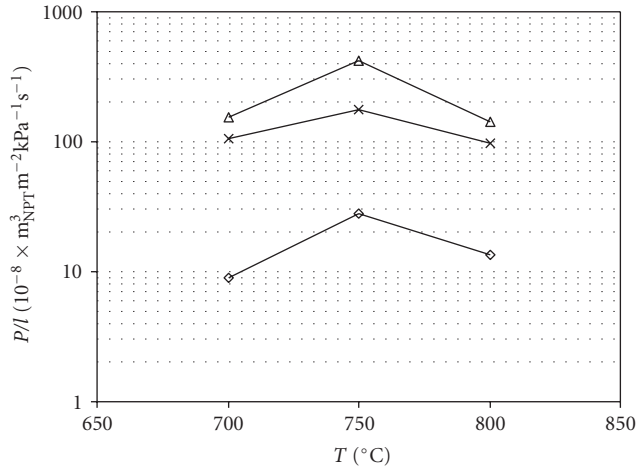

Figure 6: Permeation data of carbon membranes prepared up to 700, 750, and 800°C: ◇—N_2, x—He, △—CO_2.

3.5. Soaking Time Effect. The soaking time consisted on keeping the membranes at the end temperature for a certain time interval, just before quenching. The effect of such a soaking time on the performance of carbon membranes is presented in Table 5.

In this case, from Table 5, all the permeances are enhanced by the existence of a final isothermal step at 700°C end temperature, but all the selectivities are lower. In fact, it can be seen in Figure 4 that mass loss is still occurring at this temperature. By keeping the membranes at 700°C for 2 hours, pores are enlarged, but this causes a decrease in selectivity. As expected, this decrease is more accentuated for pairs CO_2/N_2 and He/N_2, since the larger molecule N_2 is more easily penetrating the pore network. Once again, higher permeances allied to lower selectivities might be an indication that the total pore volume has increased together with the mean pore width.

3.6. CO_2 Exposure. After exposure to CO_2, a check run was performed with N_2 to assess any possible decrease in the membranes permeances. The presence of oxygenated functional groups on the surface of CMSM was reported by other authors [12–14], and the studies done in the scope of this work were to confirm the presence of such groups. CO_2 is electron-deficient and thus acts as a Lewis-acid [15]. Although the membranes are essentially carbon, there may be some oxygenated groups on the surface [26], acting as a Lewis-bases and enhancing interactions with CO_2. Hägg et al. [13] have shown that CO_2 could plug pores leading to a decrease in permeances and suggested regeneration procedures at 200°C under inert atmosphere. Nevertheless, in the present work the experiments showed no loss in permeance due to CO_2 exposure. The permeance of N_2 after CO_2 exposure matched the one obtained when the

Table 4: Quenching effect on the permeance of carbon hollow fibers.

		Permeance ($10^{-8} \times m^3_N\, m^{-2}\, kPa^{-1}\, s^{-1}$)			Ideal selectivity		
Sample	Quenching	N_2	He	CO_2	CO_2/N_2	CO_2/He	He/N_2
HF-700-A	Yes	9	107	153	18	1.5	12
HF-700-B	No	5	84	66	14	0.8	18
HF-750-A	Yes	28	176	416	15	2.4	6.4
HF-750-B	No	16	116	236	14	2.0	7.1
HF-800-A	Yes	14	97	144	10	1.5	7.0
HF-800-B	No	8	44	119	16	2.7	5.8

Table 5: Effect of soaking time on the permeance of carbon hollow fibers.

	Permeance ($10^{-8} \times m^3_N\, m^{-2}\, kPa^{-1}\, s^{-1}$)			Ideal selectivity		
Sample	N_2	He	CO_2	CO_2/N_2	CO_2/He	He/N_2
HF-700-A	9	107	153	18	1.5	12
HF-700-ST2h	16	134	180	11	1.3	8.2

membrane was virgin or fresh. This means that, if those oxygenated groups do exist in the carbon matrix, they do not interfere with the membrane's performance which means that carbon membranes done from this precursor have that advantage over the others.

4. Conclusions

The pyrolysis parameters studied in this paper influence the characteristics, and hence, the performance of the resulting carbon membranes out of P84/SPEEK. The highest permeances were obtained for the membranes submitted to an end temperature of 750°C and to quenching. The highest ideal selectivities were accomplished for the membrane submitted to 700°C and also to quenching. It was also concluded that the existence of a final soaking time, after reaching the end temperature, just before quenching, improved the permeance of the carbon membranes, but causes a decrease in selectivity. Furthermore, it was observed that the membranes quenched after reaching the end of the process revealed higher permeances than the ones naturally cooled. No decrease in the performance of the membrane due to CO_2 exposure was observed.

Acknowledgments

The work of M. Campo was supported by FCT, Grant SFRH/BD/23833/2005. The authors would like to acknowledge the funding provided by FCT within research Project POCI/EQU/60246/2004.

References

[1] J. E. Koresh and A. Sofer, "Molecular sieve carbon permselective membrane—part I: presentation of a new device for gas mixture separation," *Separation Science and Technology*, vol. 18, no. 8, pp. 723–734, 1983.

[2] J. E. Koresh and A. Soffer, "Study of molecular sieve carbons—part 1: pore structure, gradual pore opening and mechanism of molecular sieving," *Journal of the Chemical Society, Faraday Transactions 1*, vol. 76, pp. 2457–2471, 1980.

[3] S. M. Saufi and A. F. Ismail, "Fabrication of carbon membranes for gas separation—a review," *Carbon*, vol. 42, no. 2, pp. 241–259, 2004.

[4] A. F. Ismail and L. I. B. David, "A review on the latest development of carbon membranes for gas separation," *Journal of Membrane Science*, vol. 193, no. 1, pp. 1–18, 2001.

[5] P. S. Tin, Y. Xiao, and T.-S. Chung, "Polyimide-carbonized membranes for gas separation: structural, composition, and morphological control of precursors," *Separation and Purification Reviews*, vol. 35, no. 4, pp. 285–318, 2006.

[6] J. N. Barsema, J. Balster, V. Jordan, N. F. A. van der Vegt, and M. Wessling, "Functionalized carbon molecular sieve membranes containing Ag-nanoclusters," *Journal of Membrane Science*, vol. 219, no. 1-2, pp. 47–57, 2003.

[7] J. N. Barsema, N. F. A. van der Vegt, G. H. Koops, and M. Wessling, "Ag-functionalized carbon molecular-sieve membranes based on polyelectrolyte/polyimide blend precursors," *Advanced Functional Materials*, vol. 15, no. 1, pp. 69–75, 2005.

[8] C. Liang, G. Sha, and S. Guo, "Carbon membrane for gas separation derived from coal tar pitch," *Carbon*, vol. 37, no. 9, pp. 1391–1397, 1999.

[9] A. F. Ismail and L. I. B. David, "Future direction of R&D in carbon membranes for gas separation," *Membrane Technology*, vol. 2003, no. 4, pp. 4–8, 2003.

[10] A. Soffer, M. Azariah, A. Amar, et al., "Method for improving the selectivity of carbon membranes by carbon chemical vapor deposition," US Patent no. 5695818, 1997.

[11] A. Soffer, J. Gilron, S. Saguee, R. Hed-Ofek, and H. C. Topic, "Process for the production of hollow carbon fiber membranes," US Patent no. 5925591, 1999.

[12] I. Menendez and A. B. Fuertes, "Aging of carbon membranes under different environments," *Carbon*, vol. 39, no. 5, pp. 733–740, 2001.

[13] M.-B. Hägg, J. A. Lie, and A. Lindbråthen, "Carbon molecular sieve membranes: a promising alternative for selected industrial applications," *Annals of the New York Academy of Sciences*, vol. 984, pp. 329–345, 2003.

[14] S. Lagorsse, F. D. Magalhães, and A. M. Mendes, "Aging study of carbon molecular sieve membranes," *Journal of Membrane Science*, vol. 310, no. 1-2, pp. 494–502, 2008.

[15] P. Raveendran, Y. Ikushima, and S. L. Wallen, "Polar attributes of supercritical carbon dioxide," *Accounts of Chemical Research*, vol. 38, no. 6, pp. 478–485, 2005.

[16] S. Lagorsse, M. C. Campo, F. D. Magalhās, and A. M. Mendes, "Water adsorption on carbon molecular sieve membranes: experimental data and isotherm model," *Carbon*, vol. 43, no. 13, pp. 2769–2779, 2005.

[17] T. Visser, G. H. Koops, and M. Wessling, "On the subtle balance between competitive sorption and plasticization effects in asymmetric hollow fiber gas separation membranes," *Journal of Membrane Science*, vol. 252, no. 1-2, pp. 265–277, 2005.

[18] T. Visser, N. Masetto, and M. Wessling, "Materials dependence of mixed gas plasticization behavior in asymmetric membranes," *Journal of Membrane Science*, vol. 306, no. 1-2, pp. 16–28, 2007.

[19] M. Ottaway, "Use of thermogravimetry for proximate analysis of coals and cokes," *Fuel*, vol. 61, no. 8, pp. 713–716, 1982.

[20] J. Barsema, *Carbon membranes: precursor, preparation, and functionalization*, Ph.D. thesis, University of Twente, Enschede, The Netherlands, 2004.

[21] H. C. Foley, "Carbogenic molecular sieves: synthesis, properties and applications," *Microporous Materials*, vol. 4, no. 6, pp. 407–433, 1995.

[22] Y. Xiao, Y. Dai, T.-S. Chung, and M. D. Guiver, "Effects of brominating Matrimid polyimide on the physical and gas transport properties of derived carbon membranes," *Macromolecules*, vol. 38, no. 24, pp. 10042–10049, 2005.

[23] P. S. Tin, T.-S. Chung, Y. Liu, and R. Wang, "Separation of CO_2/CH_4 through carbon molecular sieve membranes derived from P84 polyimide," *Carbon*, vol. 42, no. 15, pp. 3123–3131, 2004.

[24] F. Celso, R. S. Mauler, and A. S. Gomes, "Estudo das propriedades térmicas de filmes poliméricos compostos de speek, derivados do benzoimidazol e ácido fosfotúngstico," *Polímeros: Ciência e Tecnologi*, vol. 18, no. 2, pp. 178–186, 2008.

[25] J. E. Koresh and A. Soffer, "The carbon molecular sieve membranes. General properties and the permeability of CH_4/H_2 mixture," *Separation Science and Technology*, vol. 22, no. 2-3, pp. 973–982, 1987.

[26] J. K. Brennan, T. J. Bandosz, K. T. Thomson, and K. E. Gubbins, "Water in porous carbons," *Colloids and Surfaces A*, vol. 187-188, pp. 539–568, 2001.

Hindawi Publishing Corporation
International Journal of Chemical Engineering
Volume 2009, Article ID 563420, 7 pages
doi:10.1155/2009/563420

Research Article

Influence of Different Cations of N3 Dyes on Their Photovoltaic Performance and Stability

Luísa Andrade,[1] Shaik M. Zakeeruddin,[2] Mohammad K. Nazeeruddin,[2] Helena Aguilar Ribeiro,[1] Adélio Mendes,[1] and Michael Graetzel[2]

[1] *Laboratory for Process, Environment and Energy Engineering (LEPAE), Department of Chemical Engineering, Faculty of Engineering, University of Porto, 4200-465 Porto, Portugal*
[2] *Laboratory of Photonics and Interfaces, Institute of Chemical Sciences and Engineering, Swiss Federal Institute of Technology, 1015 Lausanne, Switzerland*

Correspondence should be addressed to Shaik M. Zakeeruddin, shaik.zakeer@epfl.ch

Received 16 October 2008; Accepted 13 January 2009

Recommended by Eugénio C. Ferreira

The N3 dye was modified by substituting two of its protons by potassium or sodium cations. The performance and stability of dye-sensitized solar cells incorporating the new dyes were evaluated under light soaking ($1000\,W \cdot m^{-2}$) at 50°C. Photocurrent measurements demonstrated that proton substitution by potassium cations rends the system more stable. Further characterization of the potassium-based devices was performed by electrochemical impedance spectroscopy to investigate the charge-transfer phenomena occurring at the different interfaces of the cells.

1. Introduction

Nowadays, a particular interest in the development of alternative energy sources arises, especially motivated not only by the need of reducing the dependency on fossil fuel resources, but also for providing the reduction of the CO_2 emissions. An attractive strategy to overcome the present energy problem is using renewable energy sources, such as the direct solar radiation, for producing clean energy. In this sense, the direct conversion of sunlight into electricity by means of photovoltaic systems makes an important contribution to this energy contend in an environmentally friendly way [1, 2]. In conventional solar cells, the charge separation occurs at the interface of two materials of different conduction mechanisms, exploiting the photovoltaic effect [3]. More recently, a new generation of cells emerged, the dye-sensitized solar cells (DSCs). DSCs are considered very promising since they use low cost, abundant and environmentally safe raw materials, showing relatively high-energy efficiency [4].

A DSC is made of a nanoparticulated titania film coated with an adsorbed dye monolayer. This thin film is applied on a glass substrate coated with a transparent conducting oxide (TCO) that collects the photoinjected electrons. A back electrode consists of the same conducting glass coated with platinum. This serves as a catalyst for the redox reaction occurring in the electrolyte present in between the two electrodes (Figure 1).

In DSCs, the dye is a crucial component to achieve high overall photoelectric conversion efficiency. Up to now, ruthenium complexes have been widely investigated due to their advantageous spectral properties, device photostability and high conversion efficiency [5–7]. An example of these ruthenium polypyridine complexes with better performance as sensitizer is the cis-di(thiocyanato)bis(4,4′-dicarboxilic acid-2,2′-bipyridine)ruthenium(II), commonly known as N3 [8]. Since the development of the N3 dye in 1993 [8], its tetrabutylammonium (TBA) salt N719 has been used as the standard red dye because of its unmatched performances. Similarly to the N719 dye, new dyes were developed bearing in mind that the number of protons in the dye influences the open-circuit potential and the short circuit current of the DSC [9]. In this work we modified the N3 dye by partially substituting its protons with different cations, namely, sodium and potassium. The modified dyes were subsequently incorporated in final DSC devices, which

were then submitted to accelerated thermal/light soaking aging tests for performance and stability evaluation. The cells were subjected to full sunlight irradiation at 50°C for about 1000 hours, during which time their photovoltaic parameters were periodically monitored.

Electrochemical impedance spectroscopy (EIS) was used to investigate the charge transfer phenomena occurring at the different interfaces of the DSCs. This technique has been widely used for the characterization of several electrochemical systems and, in particular, to analyze internal resistances in the DSCs [10–19]. In 2000 Bisquert et al. applied their models in the analysis of the mechanisms of electron recombination in nanoporous TiO_2 dye-sensitized solar cells [18]. After this first approach, EIS became more and more useful, playing a crucial role in what concerns modeling and understanding the complex charge phenomena occurring in DSCs [10–19]. The charge-transfer resistance at the TCO layer, the charge-transfer resistance at the counter-electrode/electrolyte interface, and the charge-transfer resistance at TiO_2/dye/electrolyte interface can therefore be obtained by fitting the EIS results to appropriate equivalent electrical circuits [20].

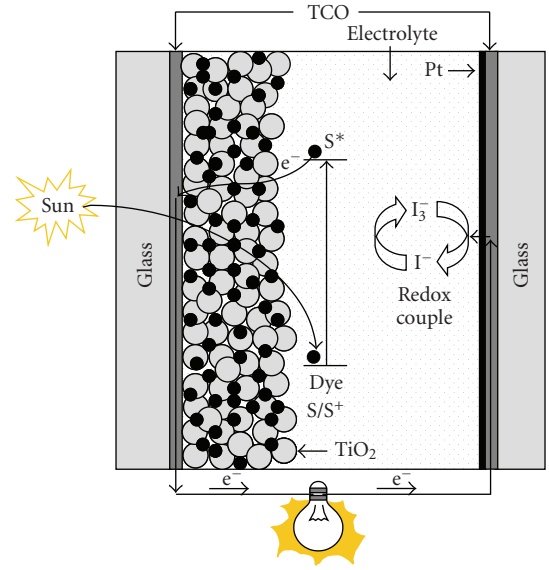

Figure 1: Schematic representation of a dye-sensitized solar cell.

2. Experimental Section

2.1. Dye Preparation. N719 dye was synthesized as reported earlier [21]. The dipotassium [$2K^+$(N3, $2H^+$)] and disodium [$2Na^+$(N3, $2H^+$)] dyes were prepared as follows. First, N719 dye was dissolved in acetonitrile solvent and to this an excess amount of potassium triflate or sodium triflate in acetonitrile was added. Immediately, the triflate counter ion was precipitated, filtered and washed with acetonitrile and dried under vaccum.

2.2. Composition of Electrolyte E1. 0.1 M iodine, 0.5 M N-methylbenzimidazole in a mixture of BMII; PMI TFSI; γ-BL (2; 3; 1) vol/vol.

2.3. TiO_2 *Electrode Preparation.* A screen-printed double layer film of interconnected TiO_2 particles was used as mesoporous negative electrode. A 7-μm thick film of 20-nm-sized TiO_2 particles was first printed on the fluorine-doped SnO_2 conducting glass electrode and further coated by a 5-μm thick second layer of 400-nm-sized light scattering anatase particles. The detailed preparation procedures of TiO_2 nanocrystals, pastes for screen-printing and double-layer nanostructured TiO_2 film have been reported elsewhere [22].

2.4. Dye-Sensitized Solar Cell Fabrication. The working electrode, described above, was sealed to the counter electrode (FTO glass—15 Ω/square—coated with a platinum solution chemically deposited at 450°C for 15 minutes) by means of a 25 μm-thick transparent Surlyn ring (from DuPont) at 130°C for 15 seconds. The cells were filled with an electrolyte solution through a predrilled hole in the counter electrode. The hole was then sealed with a Bynel disc and a thin glass to avoid leakage of the electrolyte.

2.5. Photovoltaic Measurements. All photovoltaic measurements were performed under a 450 W xenon light source able to provide 1000 $W \cdot m^{-2}$ sunlight equivalent irradiation (AM 1.5). The spectral output of the lamp was matched in the region of 350–750 nm with the aid of a Schott K113 Tempax sunlight filter (Präzisions Glas & Optik GmbH, Iserlohn, Germany) so as to reduce the mismatch between the simulated and true solar spectra. Various incident light intensities were regulated with wavelength neutral wire mesh atenuators. *I-V* curves were obtained by applying an external bias to the cells and measuring the respective photocurrent response with a digital source meter (Keithley Instruments Inc., Ohio, USA Model 2400). The incident photon-to-current conversion efficiency (IPCE) was recorded by a data-collecting system as a function of excitation wavelength. The incident light from a 300 W xenon lamp (ILC Technology, Calif, USA) was focused through a Gemini-180 double monochromator (Jobin Yvon., UK) onto the cell under test. The monochromator output was incremented through the visible spectrum to generate the *IPCE* (λ) as defined by $IPCE(\lambda) = 12400(J_{sc}/\lambda\phi)$, where λ is the wavelength (nm), J_{sc} is short-circuit photocurrent density ($mA \cdot cm^{-2}$), and ϕ is the incident radiative flux ($mW \cdot cm^{-2}$). Photovoltaic performance was determined for an active area of 0.158 cm^2 defined by a metal mask.

2.6. Electrochemical Impedance Measurements. Impedance experiments were carried out with a computer-controlled potentiostat (EG&G M273) equipped with a frequency response analyzer (EG&G M1025). The frequency range was 0.005 Hz–100 kHz and the magnitude of the modulation signal was 10 mV. All the measurements were performed at room temperature in the dark at −0.75 V bias. The EIS spectra were fitted to an appropriate electrical analogue by

means of the Z View software (v2.5b, Scribner Associates Inc, NC, USA).

2.7. Stability Tests. Hermetically sealed cells were used to check the long-term stability under visible light soaking at 50°C. The light soaking experiments employed a polymer film of 50-μm thickness (Preservation Equipment Ltd, UK), as a 400 nm UV cut-off filter. Two cells of each type with matched photovoltaic performances were exposed at open circuit to a Suntest CPS lamp (ATLAS Material Testing Solituions, GMBH, 1000 W · m^{-2}, 50°C) over a period of 1000 hours. The cells were taken out at regular intervals to record the photocurrent-voltage curve.

3. Results and Discussion

Figure 2(a) shows the photocurrent density-voltage curves obtained under AM 1.5 simulated sunlight (1000 W · m^{-2}) for DSCs prepared with [2K$^+$(N3, 2H$^+$)], [2Na$^+$(N3, 2H$^+$)], and N719 dyes in association with electrolyte E1. The cells were labelled as device A, B and C, respectively. For simplicity, the results for one single cell of each type are presented hereafter.

Comparing the three systems under study, device C shows the best initial photovoltaic performance. In fact, it is already known by its unmatched performance. On the basis of cations' substitution in the N3 dye, the anchoring groups of the adsorbed sensitizer transfer most of its protons to the semiconductor surface, charging it positively. This change in the TiO_2 surface enhances the adsorption of the anionic ruthenium complexes and favors electron injection from the excited state of the dye into the conduction band of the semiconductor, resulting in higher photocurrents. Nevertheless, this positive shift of the Fermi level induced by surface protonation leads to a low open-circuit potential. In fact, if the sensitizer has less protons, it is expected to obtain high open-circuit potential and low photocurrents, and the other way round if the sensitizer is fully protonated. So, an optimal degree of protonation of the sensitizer should be considered to reach maximum overall conversion efficiency [9]. In this study we observed that the sodium-based system (device B) presents higher values of short-circuit current, J_{sc}, and open-circuit voltage, V_{oc}, than cells with the potassium-based system (device A)—Figure 2(a). However, the latter system has higher overall power conversion efficiency, η, due to a higher value of the fill factor, *FF*. This fact is explained by a reduction in the series resistance of the cell with potassium salt dye.

In Figure 2(b) the incident photon-to-current conversion efficiency (*IPCE*) for devices A, B, and C can be compared. The *IPCE* is plotted as a function of the excitation wavelength. In line with the better photovoltaic performance, device C shows the highest *IPCE*: maximum of about 67% at 530 nm. At the same wavelength, device A reaches a maximum of 54%, while device B reaches approximately 63%.

Apart from efficiency, the long-term stability is also a key issue regarding the industrial development and commercialization of DSCs. Thus, an intimate relation between photovoltaic performances and stability should be achieved. The evolution of the photovoltaic performances throughout the aging process of the three systems under study is presented in Figure 3. Device A reveals a very good stability when compared with the two other systems. Actually, this device kept close to 90% of its initial performance after 1000 hours of light soaking at 50°C. In contrast, devices

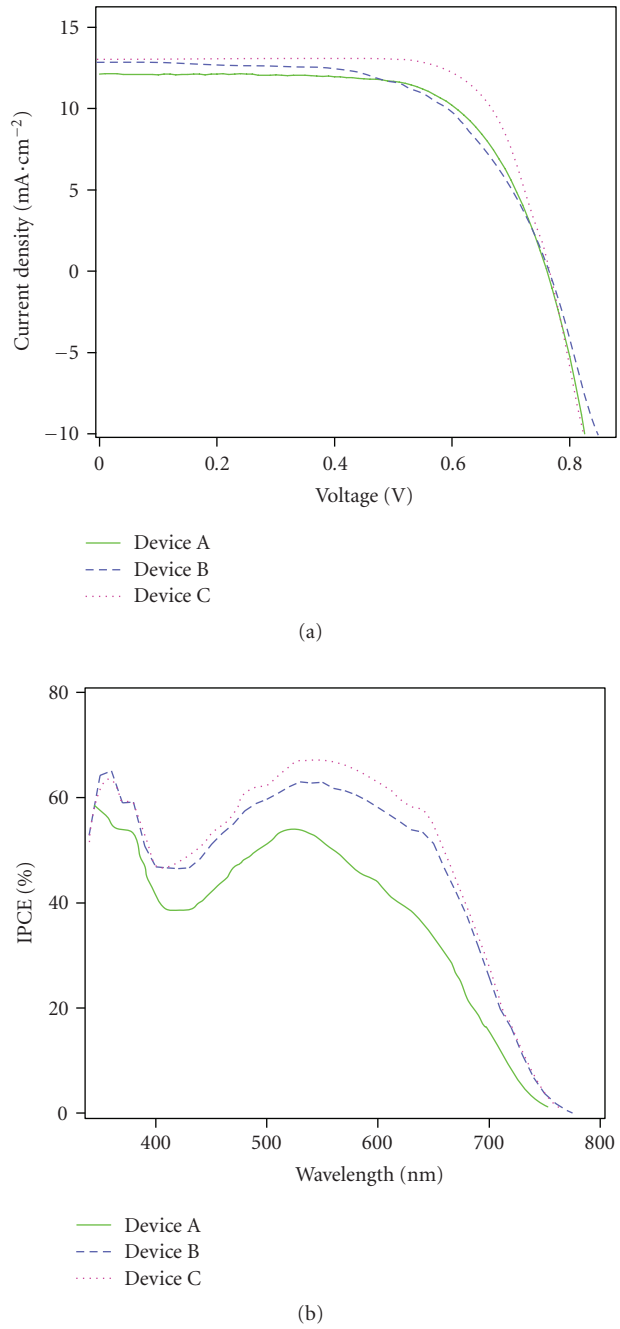

Figure 2: (a) Photocurrent intensity-voltage characteristics for devices A, B, and C, measured at 1 sun (1000 W · m^{-2}), AM 1.5 global sunlight illumination. (b) Photocurrent action spectra of the same devices.

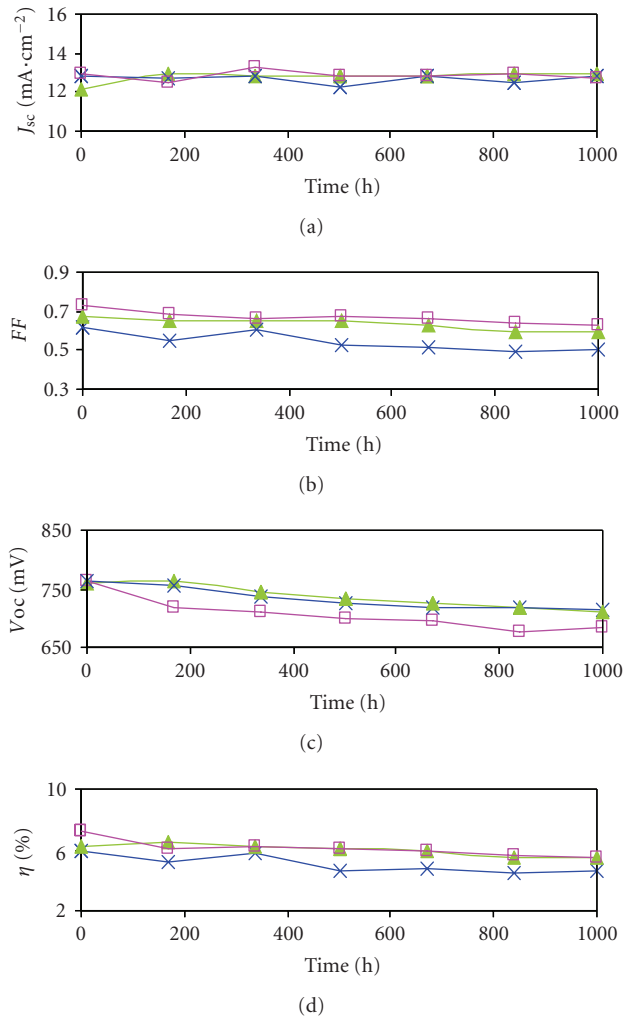

Figure 3: Evolution of photovoltaic parameters for device A (▲), device B (×), and device C (□). The cells were kept under one sun visible-light soaking at 5°C for approximately 1000 hours.

B and C showed a drop in efficiency of about 23% and 25%, respectively. The higher stability of device A is mainly due to an increase in the photocurrent (6%) during the first week of aging, which was then maintained at the same level for the rest of the aging period. Additionally, this system shows a quite stable evolution of the *FF* values, indicating constancy in series resistance during the aging process. Despite its high photovoltaic performance as a fresh cell, the N719 system was unstable, exhibiting a marked decrease in J_{sc} and V_{oc} soon after the first week. This may be due to desorption of dye from the TiO_2 surface. Moreover, the sodium salt containing device B does not rend the system very stable, as suggested by the strong oscillation in all its photovoltaic parameters.

The stability tests allow us to conclude that the number and type of substituting cations will strongly influence the photovoltaic performances of the devices. Considering the ionic potentials of the cations we can realize how strongly they will be electrostatically attracted to ions of opposite charge and to what extent the cations will repel other ions of like-charge. As the sodium cation has higher ionic potential than the potassium cation, we may be induced to say that the stability is improved when substituting the N3 protons by sodium cations. However, this conclusion is not straightforward since we have to considerer the DSC system with all its components. The present work proves this fact since potassium substitution renders a better stability. The positive shift of the Fermi level upon adsorption of the dye decreases the gap between the redox couple and the Fermi level. This fact will strongly influence the TiO_2/dye/electrolyte interaction, which is not totally understood.

Bearing in mind the promising results in terms of performance and long-term stability of the potassium-based DSC, a deeper characterization of the system was performed. In this sense, the effect of the aging process in the overall performance of device A was analyzed by means of electrochemical impedance spectroscopy. This technique allows us to determine the charge-transfer resistances at the platinum counter-electrode and at the TiO_2/dye/electrolyte interface as well as to determine the Nernstian diffusion of I^-/I_3^- ions within the electrolyte [10, 20]. The Bode and Nyquist (Z''-imaginary part of impedance versus Z'-real part of impedance) plots for the potassium-based system, before and after the aging process, are shown in Figure 4.

Several physical models have been developed in an effort to understand all the complex charge-transfer processes that take place in DSCs [15, 18, 23]. These works employ the diffusion-recombination model to study the electronic processes taking place at the semiconductor, whereas the electron transfer phenomena at the electrolyte and contact interfaces are described by simple RC electrical arrangements. Actually, the electron transport and charge recombination in nanocrystalline TiO_2 films have been widely studied by Bisquert et al. [18], who suggested an infinite transmission line model to describe the charge-transfer phenomena occurring at the mesoscopic TiO_2 film, as presented in Figure 5.

The transmission line model assumes the TiO_2 photoanode as an interconnected network where electrons, after excitation, can diffuse toward the external circuit with a resistance R_w or recombine at the TiO_2/electrolyte interface. Assuming that the recombination phenomenon is only related to electron transfer by back reaction with the electrolyte (dark current), it can be described by a charge transfer resistance, R_k, and a chemical capacitance, C_μ. If L is the thickness of the mesoscopic TiO_2 film, the electron transport resistance through the semiconductor is defined as $R_w = r_w L$, while the interfacial charge recombination resistance and the chemical capacitance at the interface are, respectively, $R_k = r_k/L$ and $C_\mu = c_\mu L$.

The other charge-transfer processes occurring in DSCs are also considered in the electrical analogue, as shown in Figure 5. Regeneration of I_3^- at the counter electrode is characterized by R_{CE} and C_{CE}, which represent the charge-transfer resistance and the double-layer capacitance at the platinized FTO glass, respectively.

Finally, the ZView software was used to fit the experimental data to the equivalent circuit presented in Figure 5. For better fitting, all capacitor elements were replaced by

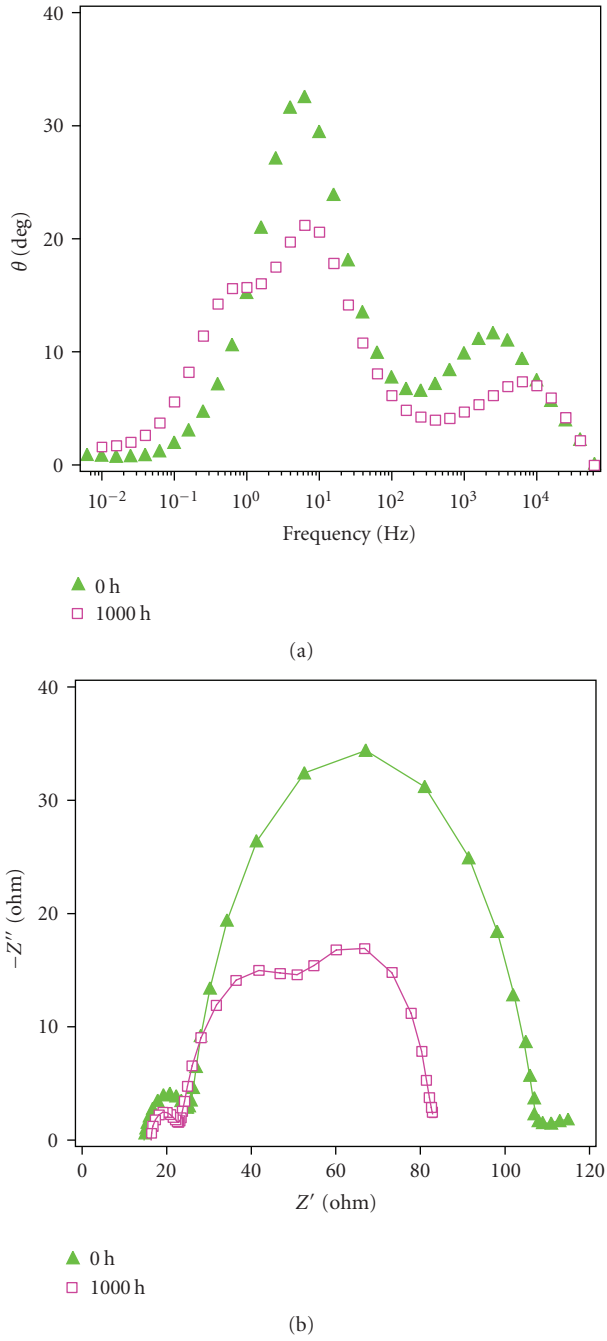

Figure 4: Bode (a) and Nyquist (b) diagrams obtained for device A before and after 1000 hours under thermal/light soaking stress. In the Nyquist diagram, symbols correspond to the impedance data obtained experimentally in the dark under −0.75 V bias, while solid lines represent the fittings according to the equivalent circuit present in Figure 5.

constant phase elements (CPEs), non-ideal capacitances associated with a nonuniform distribution of current in the heterogeneous TiO_2 film [24].

Table 1 presents some parameters useful to understand the underlying mechanisms related to the aging process. Besides R_k and R_w, the electron lifetime τ_n ($\tau_n = R_k C_\mu$),

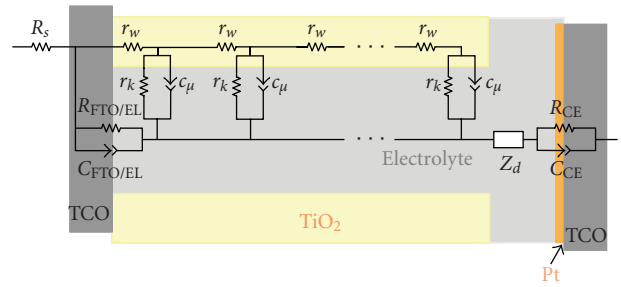

Figure 5: Transmission line model used to fit the EIS experimental data.

the effective electron diffusion length L_n ($L_n = L\sqrt{R_k/R_w}$), and the effective diffusion coefficient of electrons in the TiO_2 semiconductor D_n ($D_n = L_n^2/\tau_n$) can also be obtained [23]. According to the diffusion-recombination model, the ratio R_k/R_w ($\gg 1$) clearly shows that the charge-transfer resistance associated to recombination of electrons at the TiO_2/electrolyte interface (R_k) is much higher than the electron transport resistance through the semiconductor (R_w). This means that the cell exhibits carrier collection efficiency near unity [23].

Moreover, Table 1 shows that L_n is much higher than the thickness of the mesoscopic TiO_2 film ($L \approx 12\,\mu$m) in both fresh and aged cells, confirming the excellent transport properties. The increased J_{sc} for the aged sample can be attributed to the longer electron diffusion length compared to the fresh sample ($J_{sc}^{0\,\text{hours}} = 12.1\,\text{mA}\cdot\text{cm}^{-2}$ and $J_{sc}^{1000\,\text{hours}} = 12.9\,\text{mA}\cdot\text{cm}^{-2}$). As shown in Figure 4(a), the middle frequency peak position of the aged sample was slightly shifted to higher frequencies, revealing a decrease in the electron lifetime. The decreased electron lifetime is mainly ascribed to a major decrease in R_k (in Table 1) for the aged sample compared to the fresh one. This means that electrons recombine more easily with the electrolyte upon aging. A faster electron recapture taking place in the aged device prevents the electron accumulation in the TiO_2 nanoparticles from reaching the same density as for the fresh devices. As a result, the drop of V_{oc} was observed in aged devices (Figure 3). The same conclusions can be drawn from the significant decrease of the intermediate semicircle in Figure 4(b), which corresponds to a lower value of the charge-transfer resistance (R_k) at this interface. The increased electron diffusion coefficient was probably due to the positive shift of the conduction band energy level edge.

A decrease in the redox charge-transfer resistance at the platinum counter electrode was observed upon aging ($R_{CE}^{0\,\text{hours}} = 9.1\,\Omega$ and $R_{CE}^{1000\,\text{hours}} = 5.5\,\Omega$). This explains the decrease of the left-hand side semicircle in the Nyquist diagram. This semicircle corresponds to the high-frequency peak in the Bode plot, which has moved toward larger values (meaning lower electron lifetimes and shorter redox reaction times). Additionally, an overlap between the photoelectrode impedance (middle semicircle) and that related to the Nernstian diffusion within the electrolyte (right-hand semicircle) can be noticed. This was probably due to

Table 1: Parameters determined by fitting the EIS experimental data of device A to the equivalent circuit as shown in Figure 5.

Exposure time/hours	R_k/Ω	R_w/Ω	R_k/R_w	L_n/μm	τ_n/ms	$D_n/\text{cm}^2 \cdot \text{s}^{-1}$
0	67.2	5.1	13.3	25.5	11.1	5.90×10^{-4}
1000	32.3	1.8	18.4	30.0	4.5	2.00×10^{-3}

a larger overpotential for the I^-/I_3^- redox reaction on the platinum electrode of the aged sample, accompanied with a fill factor problem (*FF* decreases from 0.67 to 0.59 upon aging).

4. Conclusion

Two N3-based dyes were synthesized bearing in mind that the number of protons in the sensitizer influences the open-circuit potential and the short circuit current of the DSC. Potassium and sodium cations were used to substitute two protons of the N3 dye and the resulting dyes were compared with the well-known N719 dye that contains two TBA (tetrabutylammonium) cations. Despite presenting the highest initial photovoltaic performance, the N719 system was rather unstable, exhibiting a strong decrease in J_{sc} and V_{oc} upon aging, which might be due to dye desorption. In addition, sodium substitution in place of TBA does not help to enhance the stability of devices, whereas substitution with potassium salt revealed better stability compared to the other two systems. In fact, this system kept close to 90% of its initial performance after 1000 hours of light soaking at 50°C.

Acknowledgments

L. Andrade and H. Aguilar Ribeiro are grateful to the Portuguese Foundation for Science and Techonology (FCT) for their Ph.D and postdoc grants (no. SFRH/BD/30464/2006 and SFRH/BPD/36992/2007, resp.).

References

[1] M. Grätzel, "Molecular photovoltaics that mimic photosynthesis," *Pure and Applied Chemistry*, vol. 73, no. 3, pp. 459–467, 2001.

[2] K. Zweibel, J. Mason, and V. Fthenakis, "By 2050 solar power could end U.S. dependence on foreign oil and slash greenhouse gas emissions," *Scientific American*, vol. 298, no. 1, pp. 64–73, 2008.

[3] M. Grätzel, "Dye-sensitized solar cells," *Journal of Photochemistry and Photobiology C*, vol. 4, no. 2, pp. 145–153, 2003.

[4] M. Grätzel, "Photoelectrochemical cells," *Nature*, vol. 414, no. 6861, pp. 338–344, 2001.

[5] R. Amadelli, R. Argazzi, C. A. Bignozzi, and F. Scandola, "Design of antenna-sensitizer polynuclear complexes. Sensitization of titanium dioxide with $[Ru(bpy)_2(CN)_2]_2 Ru(bpy(COO)_2)_2^{2-}$," *Journal of the American Chemical Society*, vol. 112, no. 20, pp. 7099–7103, 1990.

[6] R. Argazzi, C. A. Bignozzi, T. A. Heimer, F. N. Castellano, and G. J. Meyer, "Enhanced spectral sensitivity from ruthenium(II) polypyridyl based photovoltaic devices," *Inorganic Chemistry*, vol. 33, no. 25, pp. 5741–5749, 1994.

[7] S. Ruile, O. Kohle, P. Péchy, and M. Grätzel, "Novel sensitisers for photovoltaic cells. Structural variations of Ru(II) complexes containing 2,6-bis(1-methylbenzimidazol-2-yl)pyridine," *Inorganica Chimica Acta*, vol. 261, no. 2, pp. 129–140, 1997.

[8] M. K. Nazeeruddin, A. Kay, I. Rodicio, et al., "Conversion of light to electricity by *cis*-X_2bis(2,2′-bipyridyl-4,4′-dicarboxylate)ruthenium(II) charge-transfer sensitizers (X = Cl^-, Br^-, I^-, CN^-, and SCN^-) on nanocrystalline titanium dioxide electrodes," *Journal of the American Chemical Society*, vol. 115, no. 14, pp. 6382–6390, 1993.

[9] M. K. Nazeeruddin, R. Humphry-Baker, P. Liska, and M. Grätzel, "Investigation of sensitizer adsorption and the influence of protons on current and voltage of a dye-sensitized nanocrystalline TiO_2 solar cell," *The Journal of Physical Chemistry B*, vol. 107, no. 34, pp. 8981–8987, 2003.

[10] R. Kern, R. Sastrawan, J. Ferber, R. Stangl, and J. Luther, "Modeling and interpretation of electrical impedance spectra of dye solar cells operated under open-circuit conditions," *Electrochimica Acta*, vol. 47, no. 26, pp. 4213–4225, 2002.

[11] A. N. M. Green, E. Palomares, S. A. Haque, J. M. Kroon, and J. R. Durrant, "Charge transport versus recombination in dye-sensitized solar cells employing nanocrystalline TiO_2 and SnO_2 films," *The Journal of Physical Chemistry B*, vol. 109, no. 25, pp. 12525–12533, 2005.

[12] L. Han, N. Koide, Y. Chiba, and T. Mitate, "Modeling of an equivalent circuit for dye-sensitized solar cells," *Applied Physics Letters*, vol. 84, no. 13, pp. 2433–2435, 2004.

[13] L. Han, N. Koide, Y. Chiba, et al., "Improvement of efficiency of dye-sensitized solar cells by reduction of internal resistance," *Applied Physics Letters*, vol. 86, no. 21, Article ID 213501, 3 pages, 2005.

[14] J. Bisquert, "Theory of the impedance of electron diffusion and recombination in a thin layer," *The Journal of Physical Chemistry B*, vol. 106, no. 2, pp. 325–333, 2002.

[15] M. Adachi, M. Sakamoto, J. Jiu, Y. Ogata, and S. Isoda, "Determination of parameters of electron transport in dye-sensitized solar cells using electrochemical impedance spectroscopy," *The Journal of Physical Chemistry B*, vol. 110, no. 28, pp. 13872–13880, 2006.

[16] F. Fabregat-Santiago, J. Bisquert, G. Garcia-Belmonte, G. Boschloo, and A. Hagfeldt, "Influence of electrolyte in transport and recombination in dye-sensitized solar cells studied by impedance spectroscopy," *Solar Energy Materials and Solar Cells*, vol. 87, no. 1–4, pp. 117–131, 2005.

[17] F. Fabregat-Santiago, G. Garcia-Belmonte, J. Bisquert, A. Zaban, and P. Salvador, "Decoupling of transport, charge storage, and interfacial charge transfer in the nanocrystalline TiO_2/electrolyte system by impedance methods," *The Journal of Physical Chemistry B*, vol. 106, no. 2, pp. 334–339, 2002.

[18] J. Bisquert, G. Garcia-Belmonte, F. Fabregat-Santiago, N. S. Ferriols, P. Bogdanoff, and E. C. Pereira, "Doubling exponent models for the analysis of porous film electrodes by impedance. Relaxation of TiO_2 nanoporous in aqueous solution," *The Journal of Physical Chemistry B*, vol. 104, no. 10, pp. 2287–2298, 2000.

[19] J. Bisquert, A. Zaban, and P. Salvador, "Analysis of the mechanisms of electron recombination in nanoporous TiO_2 dye-sensitized solar cells. Nonequilibrium steady-state statistics and interfacial electron transfer via surface states," *The Journal of Physical Chemistry B*, vol. 106, no. 34, pp. 8774–8782, 2002.

[20] F. Fabregat-Santiago, J. Bisquert, E. Palomares, et al., "Correlation between photovoltaic performance and impedance spectroscopy of dye-sensitized solar cells based on ionic liquids," *The Journal of Physical Chemistry C*, vol. 111, no. 17, pp. 6550–6560, 2007.

[21] M. K. Nazeeruddin, S. M. Zakeeruddin, R. Humphry-Baker, et al., "Acid-base equilibria of (2,2′-bipyridyl-4,4′-dicarboxylic acid)ruthenium(II) complexes and the effect of protonation on charge-transfer sensitization of nanocrystalline titania," *Inorganic Chemistry*, vol. 38, no. 26, pp. 6298–6305, 1999.

[22] D. Kuang, S. Ito, B. Wenger, et al., "High molar extinction coefficient heteroleptic ruthenium complexes for thin film dye-sensitized solar cells," *Journal of the American Chemical Society*, vol. 128, no. 12, pp. 4146–4154, 2006.

[23] Q. Wang, S. Ito, M. Grätzel, et al., "Characteristics of high efficiency dye-sensitized solar cells," *The Journal of Physical Chemistry B*, vol. 110, no. 50, pp. 25210–25221, 2006.

[24] J. R. Macdonal, *Impedance Spectroscopy*, John Wiley & Sons, New York, NY, USA, 2005.

Hindawi Publishing Corporation
International Journal of Chemical Engineering
Volume 2009, Article ID 273808, 5 pages
doi:10.1155/2009/273808

Research Article

The Kinetics of Ampicillin Release from Hydroxyapatite for Bones Regeneration

Giovanilton Ferreira da Silva,[1] José Sílvio Veras Albuquerque,[2] Caroliny Gomes de Oliveira,[1] Ricardo Emilio Ferreira Quevedo Nogueira,[2] and Andrea Lopes de Oliveira Ferreira[1]

[1] *Grupo de Pesquisa em Processos Biotecnológicos (GPBIO), Departamento de Engenharia Química, Universidade Federal do Ceará, Campus do Pici, Bloco 709, Pici, 60455-760 Fortaleza, Brazil*
[2] *Laboratório de Desenvolvimento de Materiais Cerâmicos (LDMC), Departamento de Engenharia Mecânica, Universidade Federal do Ceará, Campus do Pici, Bloco 720, Pici, 60455-760 Fortaleza, Brazil*

Correspondence should be addressed to Andrea Lopes de Oliveira Ferreira, andrea@ufc.br

Received 31 October 2008; Accepted 3 February 2009

Recommended by Eugénio C. Ferreira

Semisynthetic beta-lactam antibiotics are among the most used pharmaceuticals. Their use in veterinary and human medicine is in continuous expansion. There is a growing need for developing bioactive implants. Advantages of implantable drug delivery tools can include high release efficiency, precise dose control, low toxicity, and allow to overcome disadvantages connected with conventional methods. In this respect, hydroxyapatite (HA) is an elective material. It enables to produce architectures similar to those of real bones. Here we studied a kinetic model to describe ampicillin release from HA. In the course of adsorption experiment, ampicillin was dissolved, maintained at 30°C and shaken at 60 strokes/minute. Samples were withdrawn periodically for analysis and then returned to the mixture. Adsorbed amounts were measured by the difference of the concentration of the antibiotics before and after adsorption using UV adsorption at 225 nm. The aim of this work was to evaluate its application as ampicillin delivery carrier.

1. Introdution

Semisynthetic beta-lactam antibiotics are the most important class of antibacterial agents. Their use in veterinary and human medicine is in continuous expansion. Some examples of semisynthetic penicillins and cephalosporins are amoxicillin, ampicillin, cephalexin, cefadroxil, and cefazolin, among many others. They have in common the presence of the beta-lactam ring, responsible for their antimicrobial activity. They irreversibly inhibit the last step of the bacterial cell wall biosynthesis. The beta-lactam antibiotics can be described in terms of a beta-lactam nucleus with a side-chain (Figure 1).

Many different nuclei and side-chains are found in the antibiotics that are in use today. Different combinations of side-chains and nuclei form antibiotics with distinctive properties; for example, replacing the phenylacetic acid side-chain of penicillin G with D-phenylglycine (PG) results in the beta-lactam antibiotic ampicillin (Figure 2), which in contrast to penicillin G, is orally stable [1–4]. Ampicillin (6-[2-amino-2-phenylacetamide] penicillanic acid) is in the penicillin group of which penicillin proper was the first antibiotic to be used in therapy [5, 6]. It is one of most widely used semisynthetic beta-lactam antibiotics [7]. It has an estimated market of 20000 ton/year [5].

There is a growing need for developing bioactive implants, due biomaterials are biocompatible, resorbable, and present osteoconductive properties. It is known that the use of bone substances has many inherent disadvantages in practical applications, and it is linked to many surgical problems [8].

Advantages of implantable drug delivery tools can include high release efficiency, precise dose control, low toxicity, and allow to overcome disadvantages connected with conventional methods [9]. In this respect, hydroxyapatite (HA) is an elective material. It enables to produce

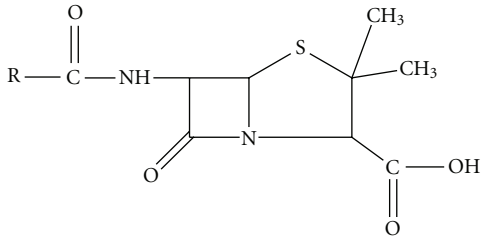

Figure 1: General structure of beta-lactam antibiotics.

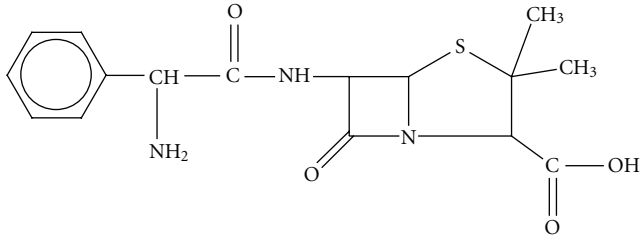

Figure 2: Structure of ampicillin, in highlighted: beta-lactam ring.

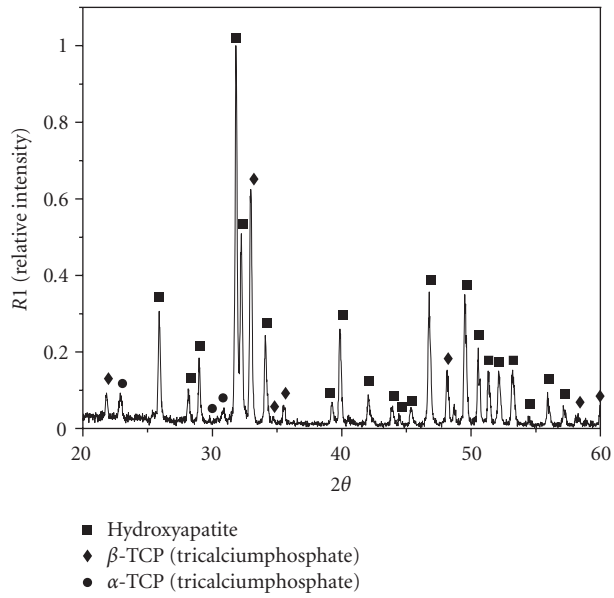

Figure 3: X-ray diffraction of HA pellet synthesized at 1350°C.

architectures similar to those of real bones. Here we studied a kinetic model to describe ampicillin release from HA. HA analogous to the mineral component of bones, its properties make it desirable as implant materials and delivery agents of drugs. This paper describes the ampicillin adsorption and release profiles of HA material. The aim of this work was to evaluate its application as ampicillin delivery carrier.

2. Materials and Methods

2.1. Materials. Ampicillin was from Aldrich Chem. Co., USA. All other chemicals were of laboratory grade from different commercial suppliers.

2.2. Antibiotic Loaded HA Samples. Ampicillin was used as drug molecules. HA were impregnated with 25 mM of antibiotic buffer solution at 30°C for 48 hours. Ampicillin adsorbed in the HA has been quantified by spectophotometric analysis. In the course of the release experiment, ampicillin was dissolved in phosphate buffer to make a stock solution, maintained at 30°C and shaken at 60 strokes/minute. Kinetic experiments to determine the amount of ampicillin adsorbed as a function of contact time were conducted by stirring. Samples were withdrawn periodically for analysis and then returned to the mixture. Adsorbed amounts were measured by the difference of the concentration of the antibiotics before and after adsorption using UV adsorption at 215 nm.

2.3. HA Synthesis. HA was synthesized by the aqueous precipitation method from CaO and H_3PO_4 as the reagents, and used as a carrier for charging ampicillin. In this study, apatite nanoparticles were produced by aqueous precipitation. The starting solution was 0.3 M H_3PO_4, 0.5 M $Ca(OH)_2$, and 1 M CH_3CHCO_2HOH. The pH value of the solution was

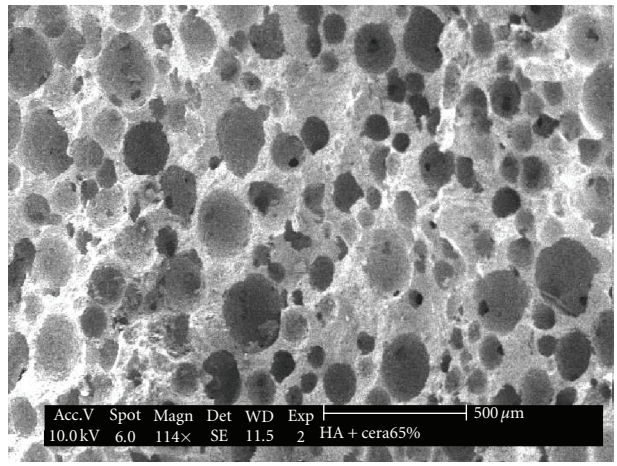

Figure 4: Scanning electron micrographs of a sample HA particle, after synthesis assay.

adjusted to pH 8 by NH_4OH additon. The suspensions were left overnight for ageing. The suspension was then vacuum filtered and washed in deionised water to remove NH_4OH. The powders were dried in an oven at 100°C overnight. HA powders and carnauba wax were synthesized in stirred 50°C. HA powders were then synthesize by means of uniaxial pressing (40 MPa) and convenient thermal treatments. The pellets were heated to 550°C to remove all wax. Pellets of cilinder shape were produced with size of 19 mm of diameter and 19 mm of length at 1350°C The powders were analyzed by X-ray diffraction (XRD) and then sintered. Sintered powders were again analyzed by XRD and scanning electronic microscopy (SEM) to assess the final phase composition [10]. Figures 3 and 4 show XRD and SEM of HA, porous of 100 ~ 300 μm were obtained.

2.4. Solubility Experiments. Solubility of ampicillin was determined following Gude et al. [11]. The samples were prepared gravimetrically. Glass-flasks with screw caps filled with the samples were immersed into a thermostated water bath and stirred. All samples were stirred for at least 4 hours. Subsequently, the mixture was allowed to settle. The samples were taken with syringes with an attached 0.2 μm filter to avoid entrainment of solids. The compositions of the liquid phases were analyzed by HPLC.

2.5. Analysis. Concentrations of ampicillin were determined using HPLC to analyze if antibiotic degraded during the assays: C18 column (Waters Nova-Pack, C18, 60 Å, 4 μm, 3.9 × 150 mm); eluent: 35% acetonitrile, 2‰ SDS (lauryl sodium sulphate), 10 mM H_3PO_4, 5 mM $K_2H_2PO_4$, with a flow of 1 mL/min at 25°C and $\lambda = 225$ nm.

2.6. Adsorption Performance. Ampicillin adsorption performance (AP) was defined as follows:

$$\%AP = \left(1 - \frac{C^*}{C^{\text{initial}}}\right) \times 100, \quad (1)$$

where C^* is the concentration of ampicillin (mM), and C^{initial} is the concentration of ampicillin at the beginning of the assays (mM).

3. Results and Discussion

3.1. Solubility Studies. The solubility of ampicillin was measured for pHs in the range 7.8–8.0, at 30°C. The selected range of pHs for the solubility studies was bracketed by stability of antibiotic. The obtained results, which are shown in Figure 5, are similar to the ones obtained by other authors [12–14].

Ampicillin solubility increases with the pH. This behavior can be explained by its determined values of the acid group pK (2.66) and amine group pK (7.24) and calculated of its isoelectric point (4.95). Hence, above the pH correspondent to its isoelectric point the number of ampicillin molecules with a neutral charge (which is the most insoluble form) decreases, leading to higher solubility values. This effect becomes more important for pH above 7.0.

Our aim is to perform the ampicillin adsorption with its separation from HA at 37°C, what implies to working at sorption conditions where the solubility of ampicillin (AMP) is the highest possible. Therefore, the obtained results indicate that for higher pH, the performance of the AMP release might be better. However, the best value for pH is a tradeoff between AMP solubility and temperature.

Temperature effects on the solubility of ampicillin were also evaluated by determining the compounds solubility at pH 7.0 and 8.0, at 37°C. The antibiotic solubility slightly increases at 37°C. Most of the solubility values at 37°C were around 11% higher than those at 30°C. However, operation of the system at 37°C implies too much lower adsorption rates than at 30°C. It is believed that an increase of 11% in the ampicillin solubility is not big enough to justify the operation at such a high temperature. Anyway, these experiments aimed at only indicating the range of adsorption conditions for studying the kinetic of the process.

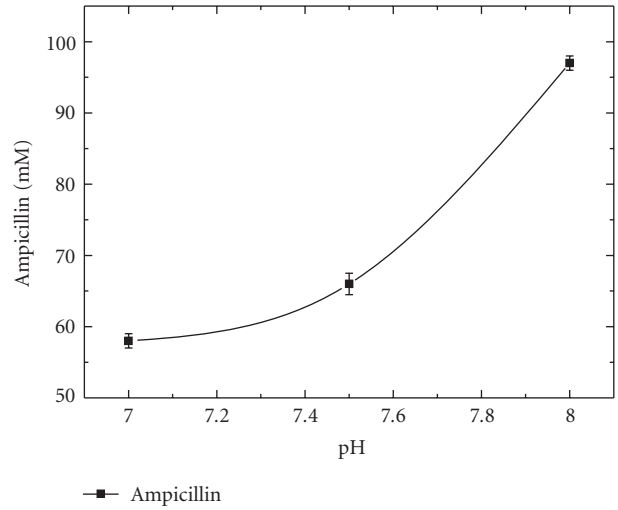

Figure 5: Solubility of ampicillin as function of pH at 30°C.

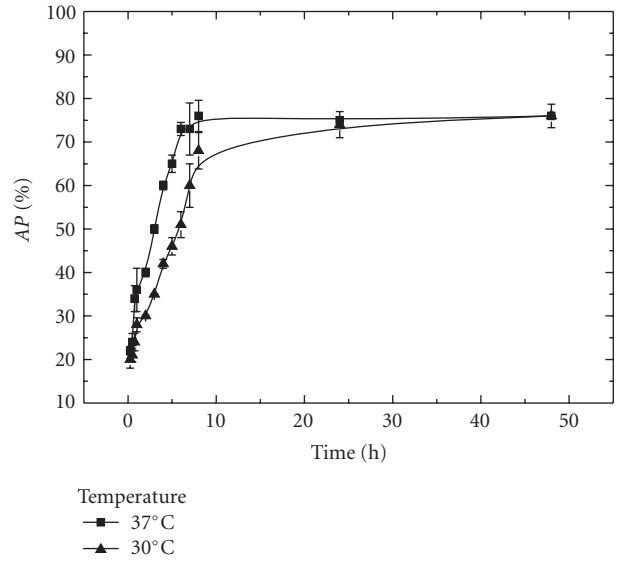

Figure 6: Equilibrium assays at $C^{\text{initial}} = 25$ mM, phosphate butter 10 mM , pH 7.5.

3.2. Equilibrium Time. In order to properly evaluate the adsorption process of ampicillin, the equilibrium curves were determined experimentally. Equilibrium time depends on adsorption rate, that is, affinity between antibiotic and HA, and temperature of assay. Figure 6 shows the results to ampicillin adsorption at 30 and 37°C, respectively. It can be observed that equilibrium state was obtained at 8 hours. At 37°C, adsorption rate higher than at 30°C can be explained due to increasing of mass transfer, because adsorption is not favor at higher temperatures.

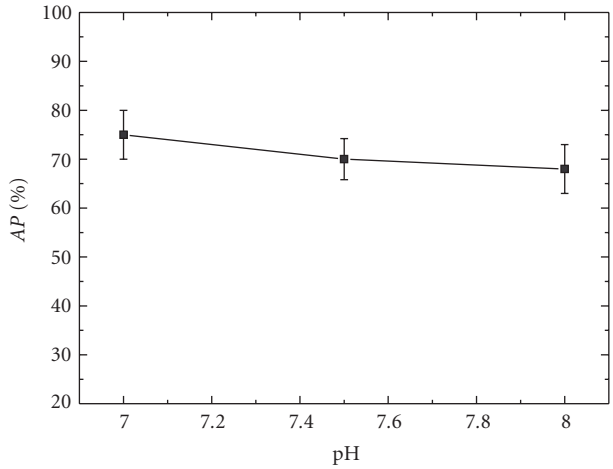

Figure 7: pH effect on adsorption ampicillin at 30°C.

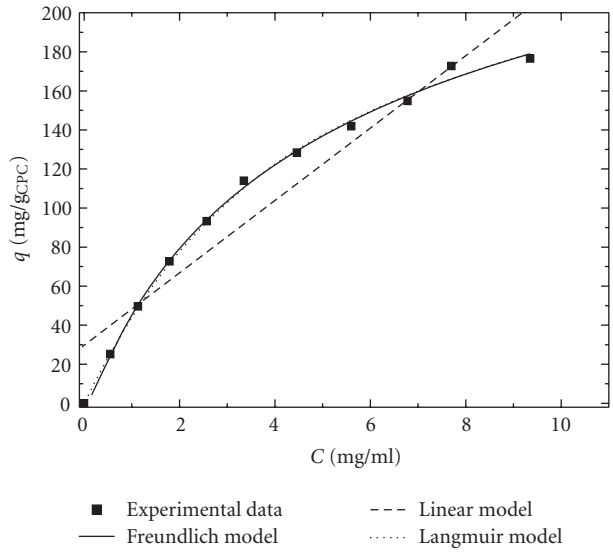

Figure 8: Adsorption isotherms of ampicillin on HA at 30°C, pH 7.0.

3.3. pH Effect at Adsorption Isotherms. Figure 7 shows the effect of pH at adsorption performance of ampicillin. It can be observed that *AP* decreases when pH increases. The amino group of ampicillin is not protoned when pH increases, so less antibiotic can be adsorbed on HA. Therefore, ampicillin adsorption slightly improves when pH decreases.

Adsorption isotherms of ampicillin on HA at 30°C and pH 7.0 were shown in Figure 8. The adsorption isotherms were further correlated to Linear, Freudlich, and Langmuir equations:

$$q = K_{\text{lin}}C,$$
$$q = K_{\text{Fr}}C^{n}, \quad (2)$$
$$q = \frac{q_m C}{K_{\text{Lan}} + C},$$

where q is the equilibrium adsorption capacity (mg/g_{HA}), C is the initial concentration of ampicillin (mg/mL), K_{lin}, K_{Fr}, and K_{Lan} are Linear, Freundlich, and Langmuir parameters, respectively. n is the Freundlich parameter related to the magnitude of adsorption driving force. q_m is the maximum adsorption capacity on HA. Some assumptions were made to adsorption model: the process operated under isothermal conditions, HA porosity was constant and homogeneous along as the particle.

The data plotted were fitted according to the Linear isotherms: $K_{\text{lin}} = 18.46 \pm 1.85$ and $R^2 = 0.958$. The Freundlich isotherms were $K_{\text{Fr}} = 52.51 \pm 3.48$, $n = 0.5688 \pm 0.036$, and $R^2 = 0.980$, and Langmuir isotherms were $q_m = 274.05 \pm 8.92$, $K_{\text{Lan}} = 4.99 \pm 0.34$, and $R^2 = 0.998$. The n value of Freundlich isotherm shows that adsorption process is favorable ($n < 1$) at 30°C. All parameters for the adsorption of ampicillin were obtained using the nonlinear least squares algorithm of Marquardt [15], with 95% confidence interval for the parameter estimates.

In the process of analysis of the models, as Freundlich isotherm and as Langmuir isotherm can represent the isotherm data of HA appropriately in the given concentration range. The Linear isotherm just presented good fitting at lower concentration. Note that a constant exist instead of zero in Figure 6, which is caused due to higher concentration of ampicillin. The best fit was obtained when Langmuir model ($R^2 = 0.998$) was used, although Freundlich model was also reached good fit.

4. Conclusions

Ampicillin solubility was studied at different pH. Higher pH improved ampicillin solubility. The equilibrium state was obtained at 8 hour of assay. At 37°C, adsorption rate was higher than at 30°C. The best results of adsorption performance were obtained when pH decreased (7.0). The relation between the adsorption capacity and the equilibrium solute concentration was analyzed. Linear, Freundlich, and Langmuir isotherms were used and provided good fit for data. The best model was achieved with Langmuir isotherm.

References

[1] M. Cole, "Penicillins and other acylamino compounds synthesized by the cell-bound penicillin acylase of *Escherichia coli*," *Biochemical Journal*, vol. 115, no. 4, pp. 747–756, 1969.

[2] M. A. Wegman, M. H. A. Janssen, F. van Rantwijk, and R. A. Sheldon, "Towards biocatalytic synthesis of β-lactam antibiotics," *Advanced Synthesis & Catalysis*, vol. 343, no. 6-7, pp. 559–576, 2001.

[3] A. Bruggink, E. C. Ross, and E. de Vroom, "Penicillin acylase in the industrial production of β-lactam antibiotics," *Organic Process Research & Development*, vol. 2, no. 2, pp. 128–133, 1998.

[4] M. P. A. Ribeiro, A. L. O. Ferreira, R. L. C. Giordano, and R. C. Giordano, "Selectivity of the enzymatic synthesis of ampicillin by *E. coli* PGA in the presence of high concentrations of substrates," *Journal of Molecular Catalysis B*, vol. 33, no. 3–6, pp. 81–86, 2005.

[5] R. A. Sheldon, F. van Rantwijk, L. M. van Langen, M. A. Wegman, L. Cao, and M. H. A. Janssen, "Biocatalysis and biocatalysis in the synthesis of β-lactam antibiotics," in *Synthesis of β-Lactam Antibiotics: Chemistry, Biocatalysis Process Integration*, A. Bruggink and P. D. Roy, Eds., pp. 102–149, Kluwer Academic Publishers, Dordrecht, The Netherlands, 2001.

[6] A. Pessina, P. Lüthi, P. L. Luisi, J. Prenosil, and Y.-S. Zhang, "Amide-bond syntheses catalyzed by penicillin acylase," *Helvetica Chimica Acta*, vol. 71, no. 3, pp. 631–641, 1988.

[7] S. Ospina, E. Barzana, O. T. Ramírez, and A. López-Munguía, "Effect of pH in the synthesis of ampicillin by penicillin acylase," *Enzyme and Microbial Technology*, vol. 19, no. 6, pp. 462–469, 1996.

[8] M. Yoshimura, W. Suchanek, T. Watanabe, B. Sakurai, and M. Abe, "Functionally graded $SrTiO_3$-$BaTiO_3$ thin films prepared by the hydrothermal-electrochemical method under flowing solution," *Journal of Materials Research*, vol. 13, no. 4, pp. 875–879, 1998.

[9] K. E. Uhrich, S. M. Cannizzaro, R. S. Langer, and K. M. Shakesheff, "Polymeric systems for controlled drug release," *Chemical Reviews*, vol. 99, no. 11, pp. 3181–3198, 1999.

[10] J. S. V. Albuquerque, J. V. F. Neto, J. I. L. A. Júnior, D. O. Lima, R. E. F. Q. Nogueira, and M. H. Prado da Silva, "Porous bioceramics produced with calcium phosphate nanoparticles," *Key Engineering Materials*, vol. 240–242, pp. 23–26, 2003.

[11] M. T. Gude, H. H. J. Meuwissen, L. A. M. van der Wielen, and K. Ch. A. M. Luyben, "Partition coefficients and solubilities of α-amino acids in aqueous 1-butanol solutions," *Industrial & Engineering Chemistry Research*, vol. 35, no. 12, pp. 4700–4712, 1996.

[12] M. B. Diender, A. J. J. Straathof, L. A. M. van der Wielen, C. Ras, and J. J. Heijnen, "Feasibility of the thermodynamically controlled synthesis of amoxicillin," *Journal of Molecular Catalysis B*, vol. 5, no. 1–4, pp. 249–253, 1998.

[13] E. S. J. Rudolph, M. Zomerdijk, K. Ch. A. M. Luyben, and L. A. M. van der Wielen, "Correlating the phase behaviour of semi-synthetic antibiotics and their precursors in water+1-butanol mixtures," *Fluid Phase Equilibria*, vol. 158–160, pp. 903–912, 1999.

[14] M. I. Youshko, L. M. van Langen, E. de Vroom, et al., "Penicillin acylase-catalyzed synthesis of ampicillin in "aqueous solution-precipitate" systems. High substrate concentration and supersaturation effect," *Journal of Molecular Catalysis B*, vol. 10, no. 5, pp. 509–515, 2000.

[15] D. W. Marquardt, "An algorithm for least-squares estimation of nonlinear parameters," *SIAM Journal on Applied Mathematics*, vol. 11, no. 2, pp. 431–441, 1963.

Hindawi Publishing Corporation
International Journal of Chemical Engineering
Volume 2009, Article ID 746439, 6 pages
doi:10.1155/2009/746439

Research Article

Drop Distribution Determination in a Liquid-Liquid Dispersion by Image Processing

Luís M. R. Brás,[1] Elsa F. Gomes,[2,3] Margarida M. M. Ribeiro,[3,4] and M. M. L. Guimarães[3]

[1] *Instituto Superior de Engenharia do Porto (ISEP), Rua Dr. António Bernardino de Almeida, 431 Porto, Portugal*
[2] *Departamento de Matemática, Instituto Superior de Engenharia do Porto (ISEP), Rua Dr. António Bernardino de Almeida, 431 Porto, Portugal*
[3] *Departamento de Engenharia de Minas, Centro de Investigac ão Geo-Ambiental e Recursos (SIPROM-CIGAR), Faculdade de Engenharia da Universidade do Porto (FEUP), Rua Dr. Roberto Frias, 465 Porto, Portugal*
[4] *Departamento de Engenharia Química, Instituto Superior de Engenharia do Porto (ISEP), Rua Dr. António Bernardino de Almeida, 431 Porto, Portugal*

Correspondence should be addressed to Elsa F. Gomes, efg@isep.ipp.pt

Received 1 October 2008; Revised 3 December 2008; Accepted 11 January 2009

Recommended by Eugénio C. Ferreira

This paper presents the implementation of an algorithm for automatic identification of drops with different sizes in monochromatic digitized frames of a liquid-liquid chemical process. These image frames were obtained at our Laboratory, using a nonintrusive process, with a digital video camera, a microscope, and an illumination setup from a dispersion of toluene in water within a transparent mixing vessel. In this implementation, we propose a two-phase approach, using a Hough transform that automatically identifies drops in images of the chemical process. This work is a promising starting point for the possibility of performing an automatic drop classification with good results. Our algorithm for the analysis and interpretation of digitized images will be used for the calculation of particle size and shape distributions for modelling liquid-liquid systems.

1. Introduction

Image processing is a very relevant area of computer science with applications in many domains. Quantitative analysis and interpretation of digitized images are currently important tools in several scientific domains.

The acquisition and treatment of images of particulate phases become essential for the calculation of particle size and shape distributions, namely in multiphase systems modelling in chemical engineering. In particular, modelling and validation of liquid-liquid systems, either for hydrodynamic or mass transfer phenomena, can benefit from image processing techniques. This is of importance in simulation, interpretation, and performance predictions of multiphase reactors. As reported in Ribeiro et al. [1], authors like Olney [2], Cruz-Pinto and Korchinsky [3] and Rod and Misek [4] have demonstrated that serious design and performance prediction errors occur if drop size distribution is neglected. According to Pacek et al. [5], any technique based on representative physical sampling will drastically change the overall composition of the dispersion.

In Ribeiro et al. [1] and Ribeiro [6] a video technique with nonintrusive probes was tested. Pictures of a small region inside a transparent vessel near its wall were obtained, by lighting and observing it from the outside. In that work, to obtain the drop size distribution, images were analyzed by employing visual/manual techniques which imply high costs, intensive labour, weariness buildup, and consequent high error rates. A fully automated computational approach has a definite potential for better performance.

The aim of the present work is to develop an algorithmic process capable of performing shape discrimination and size classification for liquid drops in monochromatic digitized frames of a liquid-liquid dispersion.

In order to automatically identify the contour of the drops, some known techniques for edge detection in images have been tested. Preliminary results with the Sobel, Marr-Hildreth, and Canny [7] methods were not satisfactory.

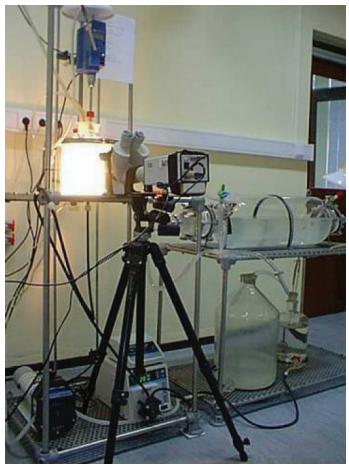

Figure 1: Experimental mixer-settler setup and image acquisition technique.

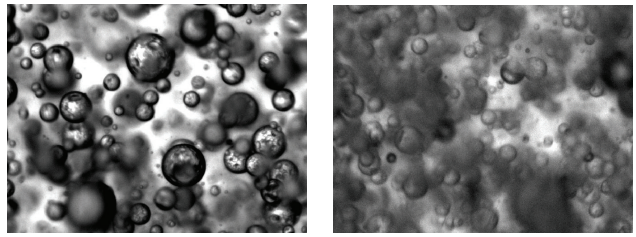

(a) (b)

Figure 2: Examples of images, (a) is a very good image, and (b) is an image with low photographic quality.

(a) (b) (c)

Figure 3: Original image, the edge detection and the detection of the drop using the Hough transform.

Therefore, we have developed a new approach which is described in this paper. After preprocessing the images, we have used Hough transforms [8] for the detection of round drops.

2. Experimental Setup and Noninvasive Image Acquisition Technique

Image frames were obtained at our SIPROM (Modelling and Simulation of Multiphase Systems) Laboratory with a digital video camera + microscope + illumination setup from a dispersion of toluene in water within a transparent mixing vessel [1] as shown in Figure 1.

The mixer consists of a 6,28 L glass vessel (diameter = height) with flat bottom, equipped with four flat vertical baffles. The agitation was provided by a standard turbine with a 1/2 turbine/vessel diameter ratio and with turbine diameter/disk diameter/paddle width/paddle height of 20/15/5/4. The mixer-settler arrangement works in closed circuit with the mixer feeds being forced in by peristaltic pumps.

For our experiments, the average residence time of the mixture in the mixer vessel was between 1 and 10 minutes, the dispersed phase hold-ups between 1 and 10%, and the agitation speed between 90 and 145 rpm.

The images were captured by a black and white SensiCam [9] camera, designed for weak lighting and fast movement (exposure times from 1 millisecond to 1000 seconds, image intervals between 0 and 1000 seconds).

Due to the high sensitivity of the camera, the lighting system had to respond to strict requirements of target ability, no flicker, high light density, low heat generation and simple and safe setup. So the light system was made up of four cool halogen lamps (150 W, 12 V each) with mirror-concentrated beam and rear cooling.

Test trials enabled the definition of the best placement of the microscope-camera group, the best placement of the lighting array and the penetration depth (up to 3 cm) into the vessel. The amplification of the combined optical image system was determined from images of a gauge made from calibrated wire immersed in the vessel. In this routine work was used a minimum frame duration (1 millisecond) in order to disable drop trails even at the highest agitation speeds. In this way, many frames (up to 1000) may be obtained per second, which enables the selection, in each frame, of only the best-defined drops without representative sample size problems.

3. Definition of the Problem

The experimental conditions (mainly phase ratio and agitation speed) led to frames of deeply focused fields with partially overlapping drops and high background noise, as we can see in Figure 2. In this figure we show two images, Figure 2(a) is what we consider a better quality image whereas Figure 2(b) is very difficult to process. Since noninvasive image acquisition and lighting were our uncompromising starting option, no significant improvements were obtained although all available image acquisition and cleaning techniques were used within this fundamental constraint. Thus, partial images and ill-defined drop boundaries led to all low cost, market-available image processing software packages requiring a high number of frames in order to secure statistically significant drop samples which, again, made for greatly time-consuming, unreliable procedures.

This led us to develop our own software for which a preliminary test and calibration stage was performed on archive images previously obtained with a semiautomated procedure [1]. We have developed a promising approach, implemented in MATLAB [10], which, given one of these photographic images of a dispersion, automatically identifies

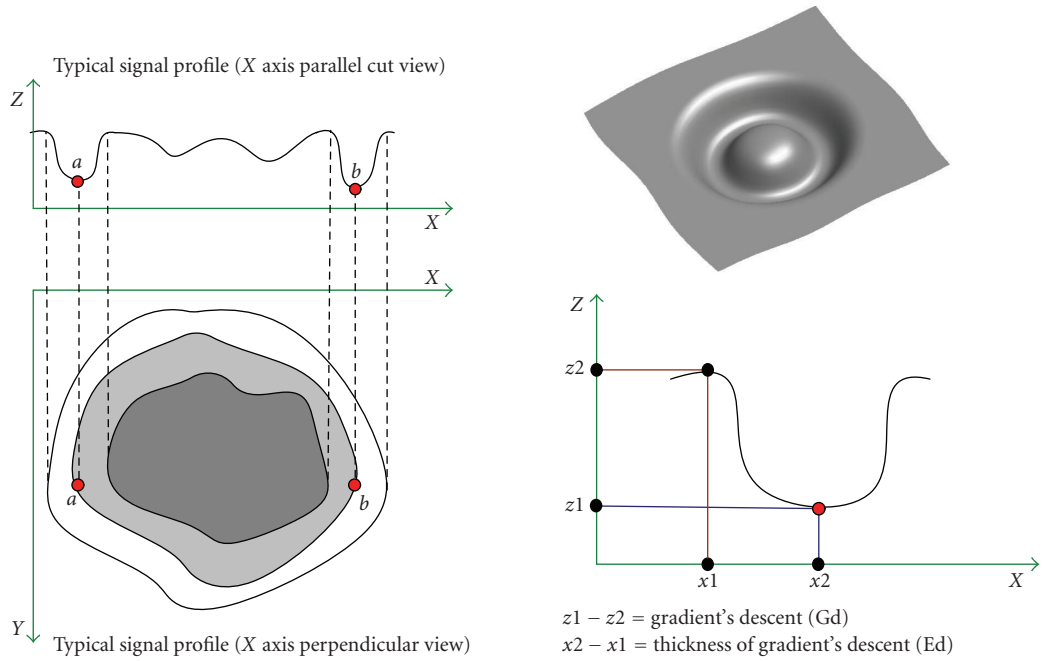

FIGURE 4: The signal profile typically presents two steep ascents and two steep descents. The algorithm uses the gradient's descent (Gd) and its respective thickness (Ed) to identify the contour of the drops.

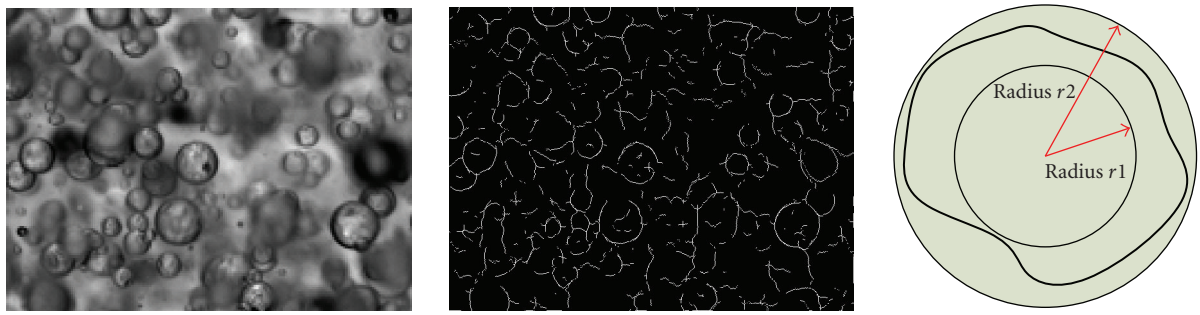

FIGURE 5: (a) Original image; (b) the resulting contour image; (c) representation of the drop contour as an irregular object.

the contour of existing drops and classifies them according to their diameter.

4. Description of the Method

Given one of the photographic images of the dispersion, our approach, implemented in MATLAB, automatically identifies the contour of existing drops and classifies them according to their diameter.

In our proposed approach, the process for the detection of the drops in an image has two distinct steps. In the first step, we detect the edges of the drops in the original image by monitoring the values of the gradient and the descending thickness and by creating an output image with those contours. In the second phase, we detect the drops in this contour image, using the Hough Transform [8, 11]. This transform is widely used in image processing to detect lines and also to detect circles.

4.1. Edges Detection. In Figure 3, we show the step of the detection process of the drops. Thus, starting from the original image (Figure 3(a)), we detect the edges (Figure 3(b)) and in the next step, we detect the contours of the drops using the Hough transform (Figure 3(c)).

In our images, of relatively poor quality, the drops have, in majority, dark edges.

To reduce the noise, and consequently reduce the probability of false edges detection, the original image (Figure 5(a)) is smoothed using a Gaussian filter. This eliminates some false contours and reduces the detection of false drops.

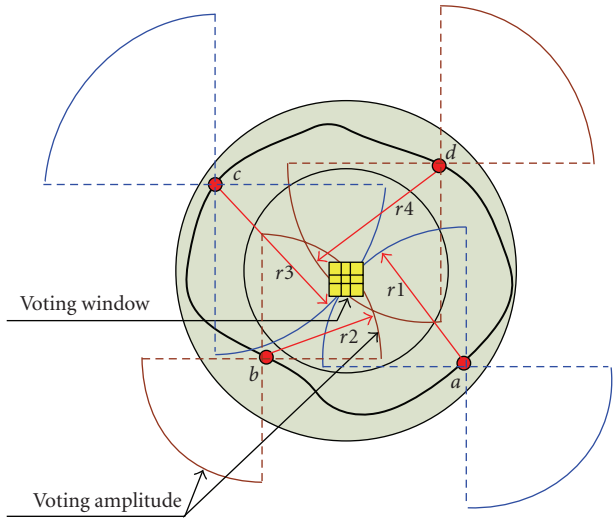

Figure 6: Voting window and voting amplitude.

Using the typical profile of the signal, edge detection is made by evaluating the relation between the gradient's descent (Gd) and its respective thickness (Ed), shown in Figure 4.

The filtered image (If) is derived, with kernels of convolution, as indicated below, originating two matrices, Ix and Iy (see (1)) corresponding to the partial derivatives dz/dx and dz/dy:

$$Ix = If * [1 \quad -1],$$
$$Iy = If * \begin{bmatrix} 1 \\ -1 \end{bmatrix}. \tag{1}$$

From the images Ix and Iy we obtain the average and the standard deviation of the descending gradient $(\mu g, \sigma g)$ and the average and the standard deviation of the descending thickness $(\mu e, \sigma e)$. The edge detection threshold is defined by the combination of Gd and Ed (computed from the Ix and Iy images), where Gd takes negative values and Ed positive.

In the processing of each descent (negative derivative) from its origin to inflexion point, if Ed $> \mu e - \sigma e/2$ and Gd $< \mu g + \sigma g/2$, then the pixel of this point is considered an edge pixel. From the matrix Ix we obtain the partial contour matrix Ia, and from Iy the matrix Ib.

Since there may be very high values of e and very low values of g, the detection of the edge pixels could be negatively affected. To reduce that possible effect we have introduced the terms $-\sigma e/2$ and $\sigma g/2$. By moving the edge detection thresholds in this way, we intend to obtain the maximally useful information without increasing significantly the risk of obtaining unnecessary information.

The sum of Ia and Ib yields the contour image Ic, shown in Figure 4. Currently, we only consider the vertical and horizontal derivatives. Taking other directions into account (such as 45 degrees derivatives) could saturate the contour detection and degrade the results. Moreover, this would increase significantly the computational effort of the method.

Preliminary experiments with other known methods for contour detection such as Sobel, Canny, and Marr Hildreth showed that these degrade the results of the Hough Transform in the detection of the drops. They introduce additional information that causes the detection of false drops.

4.2. Detection of Drops in the Contour Image. In the second step of the work, we applied the Hough transform to the contour image Ic (Figure 5(b)) to detect the contour of the drops for different values of the radius.

We consider, as we can see in Figure 5(c), that the contour of each drop can be represented as one object with irregular form, centred in a point and with a radius that varies from $r1$ to $r2$.

The Hough transform is widely used to detect lines and also to detect circles. To find circles using a Hough transform, each edge element votes for all the points x, y which are centres of the circles with radius r that it could lie on. This transform allows determining the centre of the drop through the identification of the most voted zone. It has the inconvenience of, for each useful vote, generating $2\times\pi\times r-1$ noise votes. For this reason, in an image with many drops, this could cause the detection of inexistent drops.

As referred above, in this step of the process we applied the Hough transform to the contour image Ic taking into account the relative deformation $k = (r2 - r1)/r2$ of the drops. The value of k is a parameter of the algorithm. For a maximum deformation of radius $r2$ the minimum deformation will be $r1 = r2\times(1-k)$. Votes will be generated from the successive application of the Hough Transform to the range $r1 : r2$.

This procedure is repeated for all the radii considered as maximum deformation ($r2$), in order to process all the contours, of all dimensions, of the drops (see Figure 5(c)).

The voting window (centre of Figure 6) has a dimension of 3×3 pixels for radii above 15 and dimension of 1×1 otherwise. To reduce the number of noise points we considered half of the voting amplitude (two quadrants). For that we analyze the signal of the partial derivatives according to the partial contour matrix, Ia or Ib, related to the edge pixel.

Figure 7 illustrates the detection quadrant voting procedure for an edge pixel related to matrix Ia. If the drop was a regular solid, it would be possible to determine the correct quadrant, by analyzing the gradient's angle variation, β. In our case, it is only possible to determine a pair of possible voting quadrants (A, C or B, D), by analysing the partial derivative's signal. The similar process is used for the edge pixels related to matrix Ib.

The detection process starts with the set of drops with radii between 17 and 48 pixels (0.17 and 0.48 millimeter, resp.) because these are the most frequent. Then, we treat the drops with at least 48 pixels of radius. Finally, we process the drops with radius between 8 and 16 pixels (0.08 and 0.16 millimeter, resp.).

Processing the drops with higher radius first reduces the probability of detecting false drops with a lower radius,

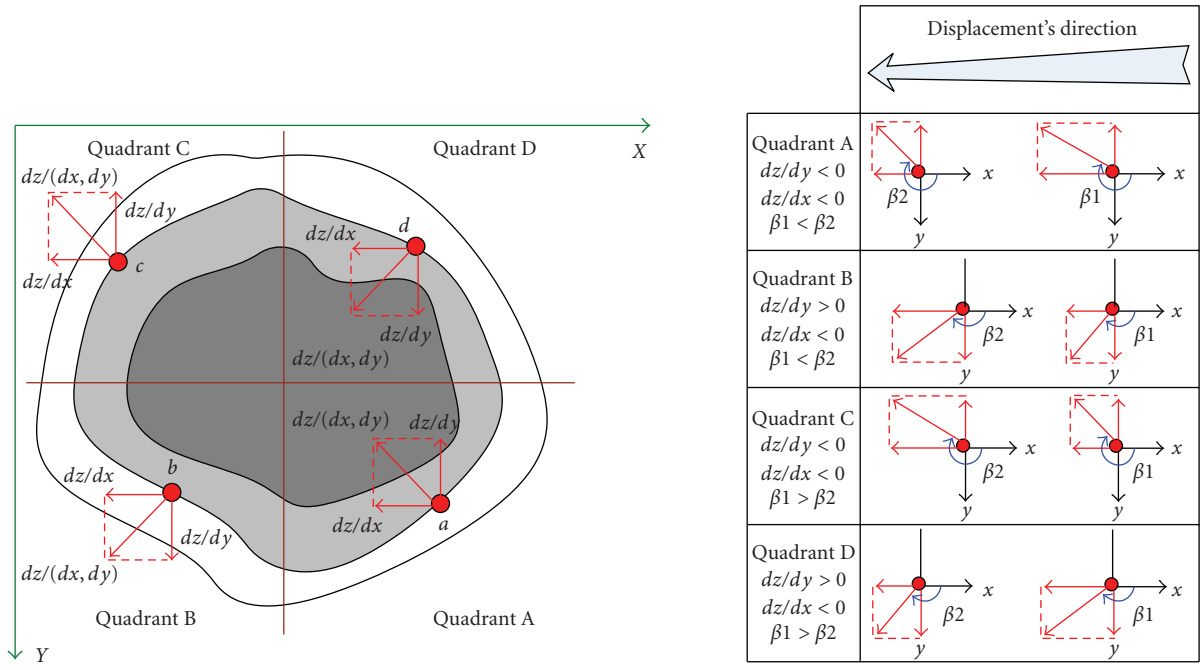

(a) (b)

Figure 7: Detection of the quadrant voting across the X axis.

Table 1: Precision and recall for different radii on two images: one pixel corresponds to 0.01 millimeter.

First image						Second image					
Radius (pixels)	Recall	Precision	Radius (pixels)	Recall	Precision	Radius (pixels)	Recall	Precision	Radius (pixels)	Recall	Precision
7	0.25	1.00	17–19	1.00	0.90	7	0.44	0.80	16	0.57	1.00
8	0.50	1.00	20	0.75	1.00	8	0.50	1.00	17	0.77	1.00
9	0.57	1.00	21	0.60	0.60	9	0.40	1.00	18	0.57	1.00
11	1.00	0.67	22	0.60	1.00	11	0.25	1.00	19	0.50	1.00
13	0.67	1.00	23	0.67	1.00	12	0.25	1.00	20	0.50	0.60
14	0.80	1.00	24	0.33	1.00	13	0.25	0.50	22	0.25	0.33
15	0.67	1.00	25-26	1.00	0.75	14	0.57	0.57	23	0.75	1.00
16	0.75	0.75	28–44	1.00	1.00	15	0.57	1.00	24–44	1.00	1.00

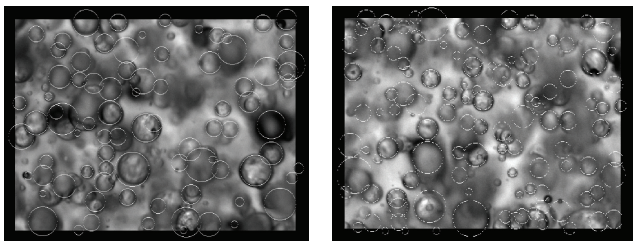

(a) (b)

Figure 8: The drops detected by our program. Each detected drop is marked with a white circle on top of the original image.

caused by agglomerates of pixels in the contour of the drops. However, the detection is not efficient for radii below 8 pixels (0.08 millimeter).

This detection process is enhanced with the erosion of the contour images of detected drops. This is not a common process of morphologic erosion [11]. In this process, after finding a centre, we eliminate the pixels that have contributed to find this centre so that they do not interfere in the subsequent process [12, 13].

In Figure 8, we can see the results obtained on two images for a radius ranging from 5 pixels (0.05 millimeter) to 46 pixels (0.46 millimeter).

5. Results

To evaluate our approach more objectively we have chosen two images with different levels of photographic quality, and compared the sets of drops obtained automatically with the drops manually identified by us. Each image

contains more than 100 drops with varying conditions (radii, overlapping, border quality, etc.). In Table 1, we show the results obtained with two of the images, the images shown in Figure 8, in terms of recall and precision values. We have calculated those values as defined in (2) where TP is the true positives (number of drops correctly identified by the program), FN the false negatives (actual drops not identified by the program) and FP the false positives (drops incorrectly identified by the program). In other words, recall measures the proportion of existing drops that the program was able to identify correctly, whereas precision is the proportion of drops identified by the program that are truly correct:

$$\begin{aligned} \text{recall} &= \frac{TP}{TP + FN}, \\ \text{precision} &= \frac{TP}{TP + FP}. \end{aligned} \tag{2}$$

In the case of the first image, we have obtained the following results. For a radius below 7 pixels the program cannot find any drop. For the radius 10 (0.1 millimeter), not in the table because recall = 0 and precision not defined, we have $TP = 0$, $FP = 0$, and $FN = 3$. For the radius 12 (0.12 millimeter), also not in the table, because recall = 0 and precision are not defined, we have a $TP = 0$, $FP = 0$ and $FN = 1$. For the other values of the radius not represented in the table, we have $TP = 0$, $FP = 0$, and $FN = 0$. As final results, taking into account all the values of radius, we have for this image a recall of 0.71 and a precision of 0.89.

For the second image, which has a lower photographic quality, we have worse results, having a total 0.55 for recall and 0.87 for precision. Nevertheless we have, for many values of radius in the image, maximum recall and precision. For several values of radius from 7 to 23 and for radius equal to 35, 40, and 45, recall and precision are not shown in the table, for the same reasons as in the previous image. We believe the cause for these worse results with respect to the previous image is the lower quality of this second image.

6. Conclusions and Future Work

In this paper, we have presented a method for the automatic identification of drops in images taken from agitated liquid-liquid dispersion. The results obtained with two images with more than 200 drops with diverse conditions (radii, overlapping, border quality, etc.) lead to the conclusion that our program is able to detect a good percentage of the drops. In the case of a better quality image, the program recognized 71% of the drops. For the other image, with lower quality, only 55% were detected. We have also observed that the approach is less efficient for smaller values of the radius, since very small drops can be easily mistaken by noise.

This work is a promising starting point for the possibility of performing an automatic drop classification with good results. However, given the limited number of images used in these experiments, these results must be further validated. Currently, we are manually identifying drops in our large library of images. Having a larger number of annotated images, we can proceed with experimental validation and further improve our results.

This can be done by fine tuning the parameters of the process, and learning the appropriate parameters given the image conditions (quality, lighting, etc.). Another line of research we are pursuing implies employing neural networks for strengthening drop recognition.

References

[1] M. M. M. Ribeiro, M. M. L. Guimarães, C. M. N. Madureira, and J. J. C. Cruz-Pinto, "Non-invasive system and procedures for the characterization of liquid-liquid dispersions," *Chemical Engineering Journal*, vol. 97, no. 2-3, pp. 173–182, 2004.

[2] R. B. Olney, "Droplet characteristics in a countercurrent contactor," *AIChE Journal*, vol. 10, no. 6, pp. 827–835, 1964.

[3] J. J. C. Cruz-Pinto and W. J. Korchinsky, "Experimental confirmation of the influence of drop size distribution on liquid-liquid extraction column performance," *Chemical Engineering Science*, vol. 35, no. 10, pp. 2213–2219, 1980.

[4] V. Rod and T. Misek, "Stochastic modelling of dispersion formation in agitated liquid-liquid systems," *Transactions of the Institution of Chemical Engineers*, vol. 60, no. 1, pp. 48–53, 1982.

[5] A. W. Pacek, I. P. T. Moore, A. W. Nienow, and R. V. Calabrese, "Video technique for measuring dynamics of liquid-liquid dispersion during phase inversion," *AIChE Journal*, vol. 40, no. 12, pp. 1940–1949, 1994.

[6] M. M. M. Ribeiro, *Measurement and interpretation of the hydrodynamical behaviour of liquid-liquid dispersions in an agitated vessel under batch and continuous flow*, Ph. D. thesis, Chemical Engineering, University of Aveiro, Aveiro, Portugal, 2002.

[7] R. J. Schalkoff, *Digital Image Processing and Computer Vision*, John Wiley & Sons, New York, NY, USA, 1989.

[8] C. R. Gonzalez and R. E. Woods, *Digital Image Processing Using MATLAB*, Prentice Hall, Upper Saddle River, NJ, USA, 2004.

[9] "SensiCam 12 bit CCD camera system," PCO AG, Donaupark 11, D-93309 Kelheim, Germany.

[10] Matlab R2006a, "The MathWorks," 2006.

[11] J. C. Russ, *Image Processing Handbook*, CRC Press, Boca Raton, Fla, USA, 2006.

[12] L. M. R. Brás, E. F. Gomes, and M. M. M. Ribeiro, "Image processing for the estimation of drop distribution in agitated liquid-liquid dispersion," in *Proceedings of the 21st International Conference on Nonlinear Science and Complexity*, J. A. Tenreiro Machado, M. F. Silva, R. S. Barbosa, and L. B. Figueiredo, Eds., Athens, Greece, July-August 2008.

[13] L. M. R. Brás, *Image processing for drop detection in a dispersion*, M.S. thesis, Electrical Engineering and Computer Science, Instituto Superior de Engenharia do Porto, Porto, Portugal, 2008.